NeuroImage: Clinical 26 (2020) 102204

Contents lists available at ScienceDirect

NeuroImage: Clinical

journal homepage: www.elsevier.com/locate/ynicl

Multi-modal normalization of resting-state using local physiology reduces changes in functional connectivity patterns observed in mTBI patients

Allen A. Champagne[a], Nicole S. Coverdale[a], Andrew Ross[b], Yining Chen[a], Christopher I. Murray[b], David Dubowitz[c], Douglas J. Cook[a,d,*]

[a] Centre for Neuroscience Studies, Room 260, Queen's University, Kingston ON K7L 3N6 Canada
[b] Performance Phenomics, 180 John St., Toronto ON M5T 1 × 5 Canada
[c] Department of Anatomy and Medical Imaging, University of Auckland, Auckland, New Zealand
[d] Department of Surgery, Queen's University, Kingston, ON, Canada

ARTICLE INFO

Keywords:
Brain connectivity
Cerebral blood flow
Mild traumatic brain injury
Resting-state fMRI
Cerebrovascular reactivity

ABSTRACT

Blood oxygenation level dependent (BOLD) resting-state functional magnetic resonance imaging (rs-fMRI) may serve as a sensitive marker to identify possible changes in the architecture of large-scale networks following mild traumatic brain injury (mTBI). Differences in functional connectivity (FC) measurements derived from BOLD rs-fMRI may however be confounded by changes in local cerebrovascular physiology and neurovascular coupling mechanisms, without changes in the underlying neuronally driven connectivity of networks. In this study, multi-modal neuroimaging data including BOLD rs-fMRI, baseline cerebral blood flow (CBF_0) and cerebrovascular reactivity (CVR; acquired using a hypercapnic gas breathing challenge) were collected in 23 subjects with reported mTBI (14.6 ± 14.9 months post-injury) and 27 age-matched healthy controls. Despite no group differences in CVR within the networks of interest ($P > 0.05$, corrected), significantly higher CBF_0 was documented in the mTBI subjects ($P < 0.05$, corrected), relative to the controls. A normalization method designed to account for differences in CBF_0 post-mTBI was introduced to evaluate the effects of such an approach on reported group differences in network connectivity. Inclusion of regional perfusion measurements in the computation of correlation coefficients within and across large-scale networks narrowed the differences in FC between the groups, suggesting that this approach may elucidate unique changes in connectivity post-mTBI while accounting for shared variance with CBF_0. Altogether, our results provide a strong paradigm supporting the need to account for changes in physiological modulators of BOLD in order to expand our understanding of the effects of brain injury on large-scale FC of cortical networks.

1. Introduction

Neuroimaging is being increasingly utilized as a tool to assess the effects of mild traumatic brain injury (mTBI) on brain health. In particular, blood oxygenation level dependent (BOLD; Ogawa et al., 1993, 1990) functional magnetic resonance imaging (fMRI) acquired at rest has highlighted that possible changes in the organization of large-scale brain networks may occur acutely and chronically following mTBI (Doshi et al., 2015; Iraji et al., 2015; Mayer et al., 2011; Nathan et al., 2015; Rosenthal et al., 2018; Sours et al., 2015; Stevens et al., 2012; Xiong et al., 2016). Functional connectivity (FC) measurements are characterized by the degree of low frequency synchronization in BOLD signal across different regions of the brain. Changes in FC have been associated with clinical recovery in injured athletes and have been suggested as a means to determine return-to-play in athletes (Lovell et al., 2007). Partial recovery of impairments in functional subnetworks have also been linked with varying degrees of compensation within cortical nodes of the brain (extending beyond a year post-injury; Dall'Acqua et al., 2017), showing that there may be differences across subjects with respect to recovery mechanisms after an mTBI.

In addition to changes in resting-state fMRI (rs-fMRI), alterations in cerebrovascular physiology have been documented following mTBI. These include changes in resting cerebral blood flow (CBF_0; Lin et al., 2016; Maugans et al., 2012; Meier et al., 2015; Militana et al., 2016; Stephens et al., 2018; Wang et al., 2018, 2016) identified using advanced arterial spin labelling (ASL) techniques (Alsop et al., 2015) and

* Corresponding author at: Department of Surgery, Queen's University, Room 232, 18 Stuart St., Kingston, ON K7L 3N6, Canada.
E-mail addresses: a.champagne@queensu.ca (A.A. Champagne), nc68@queensu.ca (N.S. Coverdale), a.ross@performancephenomics.com (A. Ross), 1yc2@queensu.ca (Y. Chen), c.murray@performancephenomics.com (C.I. Murray), dubowitz@auckland.ac.nz (D. Dubowitz), dj.cook@queensu.ca (D.J. Cook).

https://doi.org/10.1016/j.nicl.2020.102204
Received 3 September 2019; Received in revised form 2 February 2020; Accepted 3 February 2020
Available online 04 February 2020

changes in cerebrovascular reactivity (CVR; Len et al., 2011; Len and Neary, 2011; Mutch et al., 2016), characterized by the change in CBF upon exposure to a vasodilatory stimulus such as hypercapnia (HC; Fisher et al., 2018). Multiple methods exist to probe CVR clinically by inducing HC in patients including the use of a breath-hold task or an automated gas delivery system which allows control of end-tidal CO_2 partial pressures in the during an MRI scan (*reviewed in* Liu et al., 2018). Together, documented changes in CBF_0 and CVR following mTBI suggest that the symptomatic response observed in patients post-injury may be influenced by factors with vascular origins, emphasizing the need to include physiological biomarkers in the characterization of head injuries and their effects on brain health.

In studies demonstrating that BOLD rs-fMRI may serve as a sensitive marker to identify mTBI patients (Vergara et al., 2018, 2016), changes in FC are typically interpreted as impairments in neural connections between or within brain networks (if FC is lower), or evidence for brain plasticity (Bashir et al., 2012; Meehan et al., 2017) via compensatory mechanisms (if FC is higher). One limitation to BOLD rs-fMRI however is that changes in FC correlation coefficients may be confounded by changes in neurovascular coupling, defined as the changes in CBF coupled with changes in metabolic demands in response to increased neuronal activity, and baseline cerebrovascular physiology (Chu et al., 2018; Liu, 2013; Tak et al., 2015, 2014). This is because the BOLD contrast reflects a complex interplay between CBF, cerebral metabolism (via cerebral metabolic rate of oxygen consumption ($CMRO_2$)), cerebral blood volume (CBV) and venous blood oxygenation, which all contribute to the hemodynamic response that follows neural activity and modulates the local concentration of venous deoxy-hemoglobin (Davis et al., 1998; Hoge et al., 1999; Ogawa et al., 1993). Thus, factors that disturb the neurovascular coupling processes between neural fluctuations and concurrent changes in the BOLD contrast may affect the amplitude of the recorded BOLD signal fluctuations, and subsequently decrease correlation coefficients (i.e., FC measurements) between brain regions without actually changing the underlying neuronally-driven connectivity (*reviewed in* Liu, 2013; see Fig. 1). Such changes in vascular parameters have also been shown to bias the BOLD response in task-based fMRI (Bandettini and Wong, 1997; Liu et al., 2013; Para et al., 2017). In rs-fMRI, findings by (Chu et al., 2018) showed that FC measurements are dependent on a complex interaction between the BOLD signal (from neural activity) and physiological noise, which together make up the variability in BOLD measurements across the brain. It is thus critical that we consider the effects of physiological modulators of BOLD (e.g., CVR, CBF_0 and venous oxygenation) in the study of rs-fMRI, especially given that differences in vascular physiology and neurovascular coupling (A.K. et al., 2018; Burnett et al., 2014) have been documented post-mTBI.

The purpose of this paper was to introduce a multi-modal approach based on (Qiu et al., 2017) to account for local physiology in the study of rs-fMRI and FC in mTBI patients. This was done in order to explore the effects of such normalization on reported group differences in functional network architecture based on a history of mTBI. We hypothesized that multi-modal analysis of FC scaled by local physiology would reveal unique connectivity differences between the groups that may reflect differences in the organization of large-scale networks following mTBI. Altogether, our results provide a strong paradigm supporting the need to account for physiological modulators of BOLD in order to expand our understanding of the effects of disease and injury on large-scale FC of cortical networks.

2. Methods

2.1. Subjects and ethical approval

This study was approved by the Health Sciences and Affiliated Teaching Hospitals Research and Ethics Board of Queen's University (Kingston, ON, Canada). A total of 23 subjects with reported mTBI ("mTBI") were retrieved from our database. The majority of those participants presented with a history of head injury associated with sport-related concussion. Neuroimaging was obtained for patients 14.6 ± 14.9 months post-injury (range: [1–48 months]). Informed consent was obtained from each participant at the time of the MRI. Confirmation was obtained from each patient that mTBI had been diagnosed by a practicing medical professional according to the most updated International Consensus Agreement on head injuries (McCrory et al., 2013). No patients reported any loss of consciousness associated with the injury. In order to evaluate the effects of scaling FC by cerebrovascular physiology in mTBI patients, data from a control group of 27 age-matched healthy ("healthy") participants was retrieved from the same database. Healthy subjects did not report any history of mTBI and did not have positive imaging findings on the anatomical imaging. Table 1 summarized the demographic characteristics for each group.

At the time of the MRI, all subjects were asked to complete the symptom evaluation section of the Sport Concussion Assessment Tool (3rd edition; SCAT-3; Concussion in Sport Group, 2013), in order to assess for possible differences in self-rated symptoms related to mTBI between the groups (Table 1).

2.2. Structural imaging and tissue segmentation

All imaging data was acquired on a Siemens 3.0T Magnetom Tim Trio system using a 32-channel receiver head coil. A whole brain high resolution T_1-weighted magnetization prepared rapid acquisition gradient echo (MP-RAGE) image was acquired for segmentation and registration purposes with the following parameters: TR = 1760 ms, TE = 2.2 ms, time of inversion (TI) = 900 ms, voxel size = 1 mm isotropic, field of view (FOV) = 256 × 256 mm, flip angle = 9°, receiver bandwidth = 200 Hz/pixel and a total scan time of 7 min and 32 s. The 3D structural images were inspected by a practicing neurosurgeon (D.J.C.) to ensure that the anatomical image did not show any structural alterations. The anatomical scans were then brain extracted and segmented using FSL's automated 3D segmentation tool (*FAST*; Zhang et al., 2001) to create subject-specific grey-matter (GM), white-matter (WM) and cerebrospinal fluid (CSF) tissue maps.

2.3. BOLD resting-state imaging

Rs-fMRI data was acquired using a 6 min functional BOLD sequence run with a 2D echo planar imaging (EPI) readout. A total of 36 axial slices were acquired on a 68 × 68 matrix in an interleaved fashion using the following parameters: TR = 2000 ms, TE = 30 ms, voxel size = 3.5 mm isotropic, flip angle = 90°, receiver bandwidth = 2042 Hz/Px, FOV = 240 × 240 mm and no slice gap. Whole brain coverage was obtained using GRAPPA (Griswold et al., 2002) parallel imaging (acceleration factor set to 2).

2.4. Dual-echo pCASL acquisition

BOLD and CBF data were acquired simultaneously during the HC breathing protocol using a dual-echo pseudo-continuous arterial spin labelling (pCASL) sequence (Dai et al., 2008) with a 2D EPI readout and the following parameters: TR = 4000 ms, TE_1/TE_2 = 10/30 ms, FOV = 250 × 250 mm, flip angle = 90°, voxel size = 3.9 mm isotropic, slice gap = 0.773 mm, label offset = 100 mm, receiver bandwidth = 2604 Hz/pixel and EPI factor = 64. For each pCASL acquisition, the label duration was set to 1665 ms and the post-labelling delay (PLD) ranged between 1000 and 2291 ms. Because of the multi-slice single-shot EPI readout, the PLD varied across the slices acquired (average PLD = 1646 ms), which was accounted for in the computation of CBF (see below). A total of 25 axial slices were acquired on a 64 × 64 matrix (7/8 partial Fourier) in ascending order with whole brain coverage and parallel imaging (GRAPPA acceleration factor = 2).

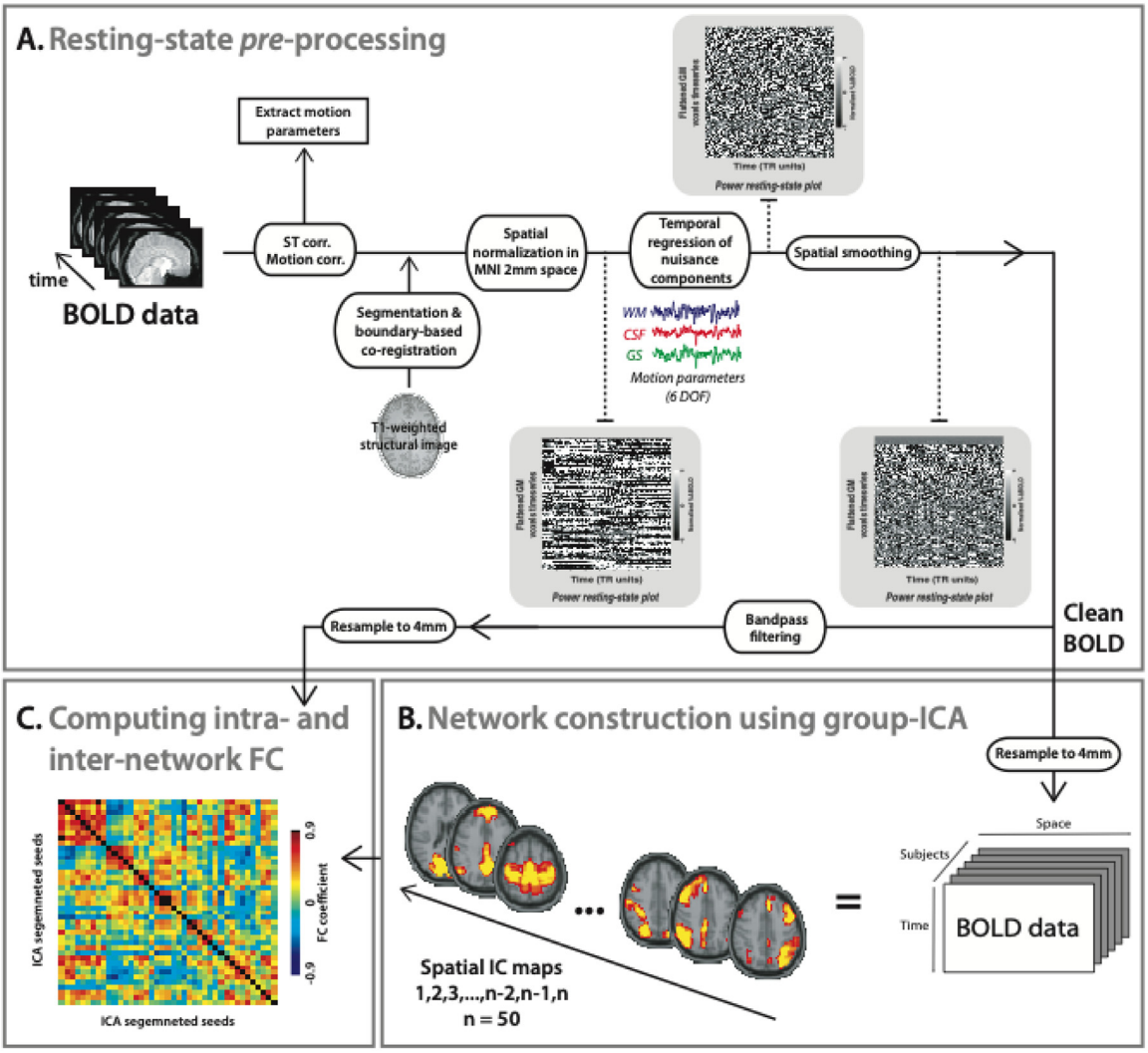

Fig. 1. Schematic summarizing the workflow for the analysis of resting-state network connectivity. (A) Pre-processing steps for the blood oxygen level dependent (BOLD) images included slice time correction (ST corr.), motion correction (motion corr.), co-registration, spatial normalization in standard Montréal Neurological Institute (MNI) space, temporal regression of nuisance parameters (white-matter (WM), cerebrospinal fluid (CSF), global signal (GS) and motion), spatial smoothing, bandpass filtering and resampling to 4 mm to align with the independent component volumes extracted in (B). The "power resting-state plots" display the time-courses of the grey-matter (GM) voxels as intensity plots for a random participant (Power et al., 2014) to show the effects of pre-processing steps employed in this study. As recommended in (V.M. et al., 2017; Vergara et al., 2017) the cleaned BOLD data was input into FSL's (Jenkinson et al., 2012) MELODIC for group independent component analysis (ICA) before bandpass filtering. A total of 50 dimensions was pre-set for the ICA with all subjects. (C) The labelled components characterized in (B) using the (Yeo et al., 2011) parcellation atlas for resting-state neural networks were used as seeds to compute intra- and inter-network functional connectivity (FC) measurements using Pearson correlations.

Table 1
Subject demographics.

	Healthy (N = 27)	mTBI (N = 23)	*P*-value[a]
Age (years)	32.2 ± 10.7	31.0 ± 11.0	0.819
Height (cm)	179.6 ± 6.6	177.5 ± 9.5	0.375
Weight (kg)	99.9 ± 45.7	107.6 ± 55.0	0.595
Number of Males (%)	20 (74)	14 (61)	N/A
SCAT-3 symptom score	2.8 ± 3.6	13.3 ± 8.0	<0.0001
SCAT-3 severity score	4.1 ± 5.6	38.6 ± 30.9	<0.0001

Values are mean ± standard deviation.
[a] = Statistically compared using a univariate ANOVA. N/A = not applicable, mTBI = mild traumatic brain injury, SCAT-3 = sport-concussion assessment tool (3rd edition).

A tissue equilibrium magnetization map (M_0) was also acquired with the same pCASL parameters, other than a longer TR (15,000 ms) and no spin labelling, for quantification of CBF.

2.5. Pre-processing of BOLD resting-state fMRI

The order of pre-processing steps in the study of mTBI has been shown to play an important role in the classification of injured subjects (Vergara et al., 2017; Vergara et al., 2017). Thus, careful steps were taken in this study to follow recommendations from (Vergara et al., 2017) in order to optimize the results of our imaging data (Fig. 1A). The first two volumes of the resting dataset were discarded to allow for the BOLD signal to reach a steady state. Following slice-time correction (Jenkinson et al., 2012a) and volume-to-volume re-alignment (*MCLFIRT*; Jenkinson et al., 2002; Mark Jenkinson and Peter Bannister, 2002), the resting BOLD EPI images were co-registered with the high-resolution T_1 image using FSL's *epi_reg* function (Jenkinson et al., 2012b) and boundary-based registration, in order to improve the alignment between the functional and structural scans (Greve and Fischl, 2009). The EPIs were then spatially normalized and transformed to the Montréal Neurological Institute (MNI) standard space using concatenated linear (*FLIRT*; 12 dof; Jenkinson et al., 2002)

and non-linear (*FNIRT*; Andersson et al., 2007) transformation matrices that aligned the functional scan to the template via the anatomical image. Temporal regression of the nuisance components including the global signal, the mean WM and CSF signals, and the six rigid-body motion parameters was done followed by spatial smoothing of each volume using a full-width at half maximum (FWHM) gaussian kernel of 6 mm. Volumes with a displacement above 0.2 mm were also censored out prior to smoothing to avoid biasing correlation coefficients based on large motion artifacts. As proposed in (Vergara et al., 2017), the smoothed data were then input into the group independent component analysis (gICA; discussed below).

2.6. Network construction and calculation of functional connectivity

Once pre-processed, each functional scan was resampled to a spatial resolution of 4mm to reduce the computational cost of the analysis (**Fig. 1B**). Resampled volumes from all subjects were then concatenated into a large 4D image and input into FSL's *MELODIC* command (Jenkinson et al., 2012a) to carry the gICA and separate the neural-related signals from different sources of noise and variability across subjects (Beckmann, 2012; Murphy et al., 2013). The resultant set of functionally independent resting-state components were first inspected visually (Griffanti et al., 2017) and overlaid onto the well-known pre-defined functional network atlas from (Yeo et al., 2011). Components with spatial correlation over 0.3 based on FSL's *fslcc* (Jenkinson et al., 2012a) tool were kept for further analysis. Spatial maps with considerable overlap with CSF or WM were automatically discarded.

A total of 6 large-scale resting networks (**Fig. 2**) were identified based on the atlas from (Yeo et al., 2011): default mode network (DMN), dorsal attention network (DAN), somatomotor network (SMN), visual network (VN), ventral attention network (VAN) and fronto-parietal network (FPN). The identified spatial components were masked to a statistical threshold set to $|t| > 4$ and then clustered into seeds to identify brain areas of relevance within each network of interest. As recommended in (Vergara et al., 2017), the pre-processed BOLD rs-fMRI image were then temporally smoothed with a Gaussian filter (approximate cutoff frequency = 0.15 Hz) before computing correlation coefficients between the seeds. Seed-based intra- and inter-network correlations were then extracted between each region's time course and all other region of interests' (ROI) timeseries, in order to create a large-scale connectivity matrix for each subject (Fig. 1C).

2.7. Voxelwise CBF_0 and CVR mapping and registration in standard space

To quantify CVR, each subject completed a 6-minute HC breathing protocol (Fig. 3A) during which the end-tidal carbon dioxide ($P_{ET}CO_2$) was targeted to 10 mmHg above baseline using a computerized feed-forward system (RA-MR^{TM}, ThornHill Research Institute, Toronto, ON, Canada) connected to a gas blending unit (Mark et al., 2010; Prisman et al., 2008). The boxcar manipulation consisted of a 2-minute baseline, followed by a block of gas inhalation (2-minute) and a 2-minute recovery period (Fig. 3A). During HC, end-tidal pressure of oxygen ($P_{ET}O_2$) was held constant at baseline values (~110 mm Hg) while the automated system sampled the partial pressures of the subject's expired air via a facemask sealed using adhesive tape (Tegaderm, 3M Health Care, St. Paul, MN, US).

The BOLD data from the pCASL acquisition during HC was used to compute CVR as the percentage change in signal divided by the change in $P_{ET}CO_2$ during the task (CVR = Δ%BOLD/ΔmmHg). The BOLD contrast was isolated from the pCASL images using a surround averaging of the second echo (TE_2 = 30 ms; Smith and Brady, 1997). Extracted volumes were motion corrected (*MCFLIRT*; Jenkinson et al., 2002; Mark Jenkinson and Peter Bannister, 2002), brain extracted (*BET*) and co-registered with the high-resolution structural image using the *epi_reg* tool (Jenkinson et al., 2012b) and rigid-body registration (6 dof; *FLIRT;* Jenkinson et al., 2002). Volumes were then smoothed with a Gaussian kernel of 8mm using *SUSAN* (Jenkinson et al., 2012b) and high-pass filtered to correct for the possible linear drift in the signal during the EPI acquisition. Following conversion of the BOLD signal to a percent change from baseline, CVR maps (Fig. 3B) were computed for each subject by averaging volumes acquired during HC (Fig. 3A) and dividing out the change in $P_{ET}CO_2$. Only the last 80s of HC (out of 120s) were used to compute the mean BOLD change in signal during the stimulus in order to avoid possible bias from delays in the vascular response to HC (Champagne et al., 2017; Donahue et al., 2016; Poublanc et al., 2015).

CBF_0 data were reconstructed from the first echo of the pCASL sequence (TE_1 = 10 ms) using a linear surround subtraction of the adjacent tag and control volumes (ΔM). Following spatial smoothing of the ASL volumes (8mm FWHM), a voxelwise CBF_0 map (mL/100g tissue/min; Fig. 3C) was computed for each subject using FSL's *oxford_asl* toolbox (Chappell et al., 2009) with partial volume (Chappell et al., 2011) and T_2* correction. This was done in order to reduce the partial volume effects from neighboring voxels containing a mixture of GM, WM and CSF. The slice-varying differences in PLD due to the 2D EPI readout were corrected using $PLD_i = 1000\text{ ms} + (s_T)*(i-1)$, where s_T represents the slice time in milliseconds (s_T = 53.8 ms). Baseline volumes prior to the stimulus (Fig. 3A) were then averaged to compute the CBF_0 maps (Fig. 3C).

Once constructed, the CVR and CBF_0 maps were aligned in standard

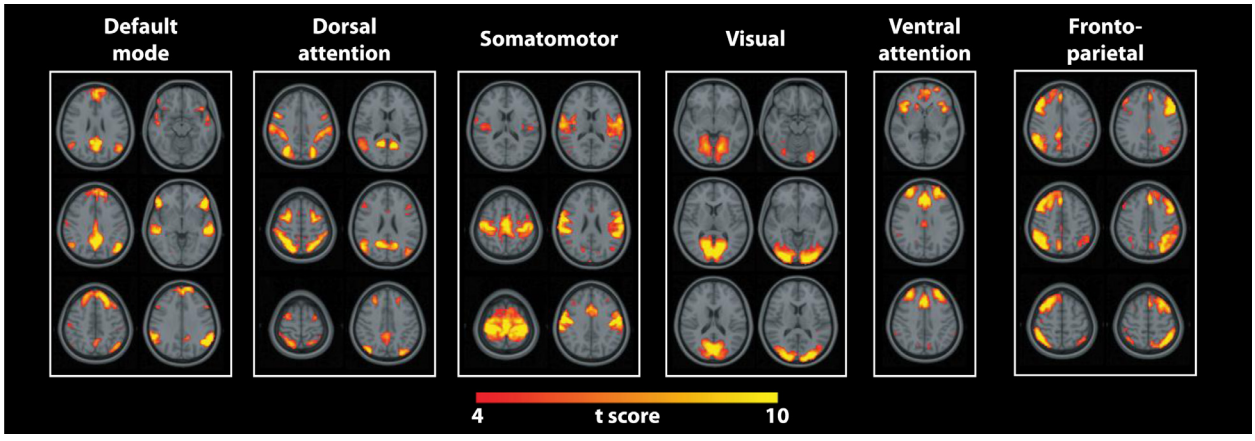

Fig. 2. Independent component analysis. Statistical results from the independent component analysis (ICA) using the resting functional data from the entire cohort and a pre-set total number of 50 dimensions. Components of interest were identified using the *fslcc* (Jenkinson et al., 2012) function combined with the (Yeo et al., 2011) parcellation atlas for resting-state neural networks. Statistical component maps (yellow-red) are overlaid onto the MNI template and threshold at a minimum t score set to 4. (For interpretation of the references to color in this figure legend, the reader is referred to the web version of this article.).

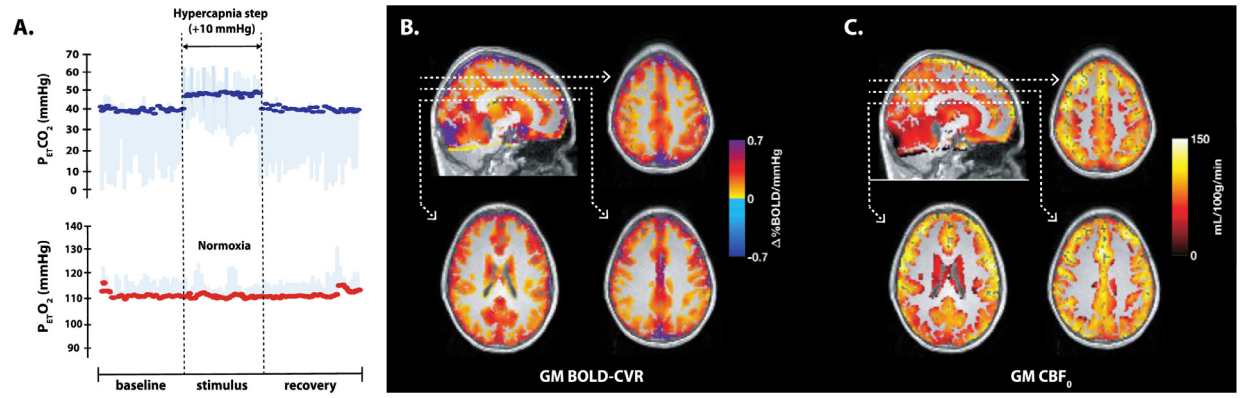

Fig. 3. Computation of voxelwise cerebrovascular reactivity (CVR) and resting cerebral blood flow (CBF_0) maps. (A) Real-time end-tidal CO_2 ($P_{ET}CO_2$; top, blue dots) and O_2 ($P_{ET}O_2$; bottom, red dots) peaks during the normoxic hypercapnia breathing manipulation. The peaks are overlaid onto the respiratory timecourse (light blue trace) targeted and collected using the RA-MR™ (ThornHill Research, Toronto, ON, Canada) computerized system. (B–C) Sample grey-matter (GM) blood oxygen level dependent (BOLD) CVR (B) and CBF_0 (C) maps in a control subject overlaid onto the high-resolution anatomical scan registered in Montréal Neurological Institute (MNI) standard space. Possible voxels including cerebrospinal fluid (CSF) were masked out to limit the partial volume effects between tissues. (For interpretation of the references to color in this figure legend, the reader is referred to the web version of this article.).

MNI space using a combination of affine (12 dof; Jenkinson et al., 2002) and non-linear warp-fields (*FNIRT;* Andersson et al., 2007) that registered the EPI functional images from native to standard space via the high-resolution structural image. Images were then resampled to 4mm isotropic voxels in order to align spatially with the rs-fMRI spatial components extracted from the gICA.

2.8. Calibration of functional connectivity coefficients using seed-based physiology

Differences in physiological modulators of the BOLD contrast (e.g., CBF_0 and CVR) post-mTBI may affect the amplitudes and correlation coefficients across regions of the brain included in large-scale networks (Chu et al., 2018; Liu, 2013; Qiu et al., 2017). To account for these confounds, we implemented a weighting scheme proposed by (Qiu et al., 2017) that adjusts seed-to-seed correlation coefficients based on local physiology (**Fig. 4**). This global scaling was applied to all seed-to-seed correlation coefficients (see below) studied *if* significant differences in the vascular parameter (i.e., CBF_0 or CVR) specific to the gICA spatial components were documented between the group at the voxelwise level (discussed next). This is because group-based differences in physiology within the gICA spatial components may contribute or bias the rs-fMRI metrics studied within the large-scale networks (Chu et al., 2018). However, if no differences in physiology were identified, no scaling for that vascular parameter was applied.

In this analysis (*see* results Section 3.2), significant group-based differences in CBF_0 spread across voxels of the large-scale network were identified. However, no significant voxelwise differences in CVR were documented suggesting that mechanisms for modulation of blood flow during HC were similar between the groups. Because network-based differences in CBF_0 were observed, individual functional connections between each seed were scaled by the seeds' mean CBF_0 measurement. This was done by multiplying the Pearson correlation coefficient ($Pearson's\ r = \rho(x_{r(seed_1)}, y_{r(seed_2)})$) by the inverse of the product of the seeds' CBF_0, normalized by the mean GM value (weight = $GM_{CBF0}/(seed_{1(CBF0)} * seed_{2(CBF0)})$; **Fig. 4**), as proposed in (Qiu et al., 2017). The resultant weighted coefficient thus reflects the degree of synchronization between two ROIs timeseries, scaled by the possible contribution of local cerebrovascular physiology (Qiu et al., 2017).

2.9. Clinical assessment of sensorimotor performance

In order to assess sensorimotor function between the groups, each

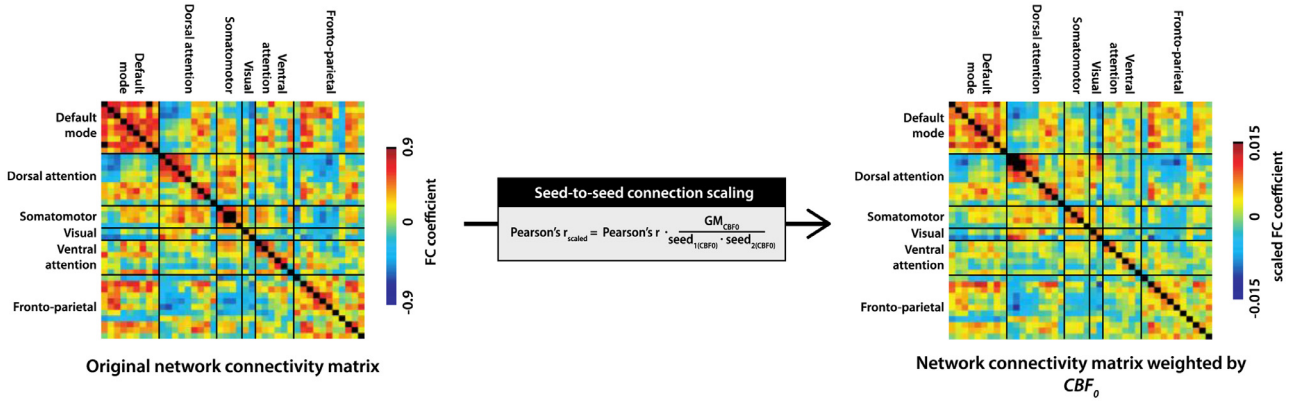

Fig. 4. Scaling functional connectivity measurements using weights derived based on local physiology. The original inter- and intra-network connectivity matrix (middle) shown in Fig. 1C derived from computing Pearson correlation coefficients (ρ) across all seeds extracted from the independent component analysis (Fig. 3). Original ρ values between seeds were normalized independently using the resting cerebral blood flow (CBF_0; right) map by multiplying the ρ index times a weight factor. The weight factor for ρ between two seeds (ROI_1 and ROI_2) was computed by dividing the mean grey-matter (GM) CBF_0 (or CVR; not shown) value by the product of the regional measurements ($ROI_1 \cdot ROI_2$), as shown on the equation above the arrow. The final resultant matrix (right) provides functional connectivity (FC) estimates that are weighted by the local physiology. This method was first introduce in (Qiu et al., 2017) to account for the possible confounding nature of changing perfusion on FC analysis within and across subjects.

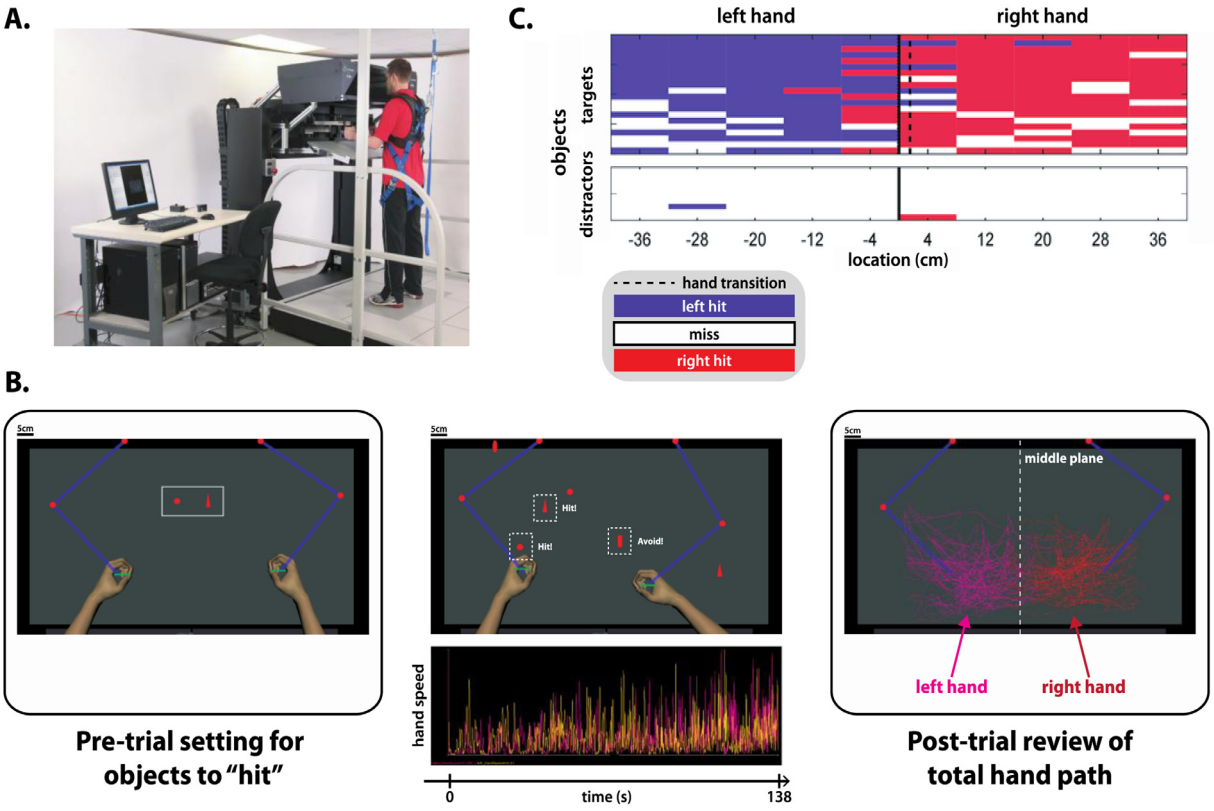

Fig. 5. Robotic assessment of sensorimotor and cognitive functions using object hitting task. (A) The KINARM end-point robot lab (BKIN Technologies, Kingston, ON, Canada). Participants are secured into the robotic arms via a harness in case of any falls from the cognitive load. The robotic arms allow for movement in the horizontal plane and in depth characterizing of sensorimotor features from the task. (B) The view of the virtual environment platform seen by the subject showing a projected version of their hands on the screen below their eyes. The subject is informed in the pre-trial setting to "hit" the red circles and triangles, while avoiding everything else (left). The shapes appear at random from 10 different bins (not displayed) at an increasing speed throughout the task (~140 s). The subject uses 5 cm paddles to hit away the shapes of interest (middle-top). Upon contact with a shape, the robot generates a 50 ms force pulse to provide feedback of contact with the object. Sensorimotor parameters like positions and velocities for each hand are recorded at a sampling rate of 1000Hz. The timeseries (middle-bottom) show the real-time recording of the hand speed for the right (pink) and left (yellow) hands. The total hand path for each hand is also shown (right). (C) Performance grid for the task where the X-axis represents the bins and the Y-axis shows the random blocks increasing in speed from top to bottom. Successful hits for the right (red) and left (blue) hands are colored respectively, while misses are shown in white. Distractor hits signify that the subject attempted to contact a shape outside of the ones selected by the robot pre-trial. (For interpretation of the references to color in this figure legend, the reader is referred to the web version of this article.).

subject completed the "object hit and avoid" task (OHA; Bourke et al., 2016) using the standing bilateral KINARM^{TM} end-point robot (BKIN Technologies Ltd., Kingston, Ontario, Canada; Fig. 5A), which creates a virtual environment platform seen by the participant (Little et al., 2015; Scott, 1999). The bilateral graspable robotic arms measure how the subject moves in the horizontal plane and applies loads to move the limb(s) in the workspace to create haptic feedback for virtual objects.

The OHA task (Fig. 5B) was designed to assess rapid bimanual motor actions, spatial and temporal performance during the task, as well as attention, executive functions and inhibitory control. Specifically, each participant is first shown a pair of target shapes to memorize (Fig. 5B left). These are the only shapes they are instructed to hit during the entire duration of the task. All other shapes are considered to be distractors and must be avoided successfully (Fig. 5B middle). A total of 300 objects are dropped from 10 bins spread across the width of the 80 cm workspace (Fig. 5B). When a target is hit using the virtual paddle, the target is pushed away and the robotic arm gives haptic feedback (i.e., small force pulse). If the participant hits a distractor, the paddle passes through the object and no haptic feedback is delivered in order to let the subject know about successful and unsuccessful maneuvers. During each trial, sensorimotor parameters such as positions and velocities are recorded for each hand at a sampling rate of 1000Hz. These are then used to compute a performance grid (Fig. 5C) and extract sensorimotor parameters that provide an index of the participant's sensory, motor and cognitive function (Table 2).

2.10. Statistical analyses

All spatial components extracted from the gICA (**Fig. 2**) were masked and merged into one image to create a large-scale network map of the voxels that were included in the characterization of seed-to-seed connectivity. This mask was then used to restrict the voxelwise group-comparison of the CVR and CBF_0 maps and determine whether cerebrovascular physiology differed between the groups within the ROIs studied. The network-specific mask used to restrict the gICA was also further filtered using the T_2* signal in order to eliminate voxels with baseline T_2* values below 30ms, which are likely caused by susceptibility artefacts (as done in Lajoie et al., 2016).

Physiological maps (i.e., CBF_0 and CVR) were assessed for significant differences between the groups using a voxel-based analysis performed in AFNI's (Cox, 1996) *3dMVM* (Chen et al., 2014). The voxelwise analyses were corrected for multiple comparisons using 10,000 Monte Carlo simulations in AFNI's *3dFWHMx* (with spatial AutoCorrelation) and *3dClustSim* (Cox et al., 2017, 2016) and a *P* value was set to 0.05. Clusters showing statistical differences between the groups were then extracted to compute the average value for the ROI in each subject and run post-hoc tests to describe the direction of the group effect.

Intra- and inter-region connectivity were compared between the groups using a series of ANOVAs corrected at a false discovery rate set to a *P* value of 0.05 (adjusted). This was repeated for normalized

Table 2
Description of sensorimotor parameters computed from the KINARM™ object hit and avoid task.

Object hit and avoid parameters	Meaning	Motor/sensory/cognitive domain targeted
Distractor hits total	Total count of distractor objects hit with both hands during the task.	motor (inhibition)
Hand bias hits	Measurement ranging between -1 (left) and 1 (right) characterizing the hand used most often to hit the objects. A value of 0 indicates equal use of both hands.	hand dominance & visuospatial bias
Median error	Percentage of the progress through the task based on the number of balls dropped (not time) when the subject makes half of their total mistakes. Higher values indicate an ability to maintain focus throughout the task.	cognitive stamina
Object processing rate	Measurement indicating the number of objects processed correctly per second at the time when 80% of the objects (240 objects) in the task have entered the screen. Higher values suggest that the participant could separate the targets and the distractors properly up to that point in the task.	sensorimotor (integration)
Target hits total	Total count of target objects hit with both hands during the task.	motor

connectivity measurements scaled by CBF_0 since group-differences were identified (*see* results Section 3.2) within voxels spread across the spatial distribution of large-scale networks studied.

All five sensorimotor parameters (Table 2) were compared between the groups using a series of univariate Analysis of Variance (ANOVA) and a significance level set with a P value < 0.05.

3. Results

3.1. Participants

This study analyzed a total of 23 mTBI subjects compared to 27 healthy controls. Groups did not differ significantly with respect to age, height or weight (Table 1). mTBI subjects reported significantly greater and more severe symptoms collected using the SCAT-3 scale (Table 1), compared to the healthy participants. Despite being more symptomatic at the time of the MRI, the studied mTBI patients did not show any significant differences in the sensorimotor parameters of the OHA task studied using the KINARM™ (Table 3).

3.2. Voxelwise differences in physiological measurements

Voxelwise analysis of the CVR maps showed no significant differences in vascular reactivity between the groups ($P > 0.05$, corrected at a cluster volume size of 33 voxels). Despite finding no differences in CVR, significant differences in baseline perfusion (i.e., CBF_0) were documented between the groups (Fig. 6; $P < 0.05$, corrected at a cluster volume size of 94 voxels). A total of three cortical clusters were identified (cluster size = 173, 228 and 293 voxels), which spread across the networks studied (Table 4). Specifically, higher baseline perfusion was observed in the mTBI group (101.8 ± 21.6 mL/100g/min), relative to the healthy participants (84.5 ± 16.5 mL/100g/min), although no direct relationship between time post-injury (in months) and CBF_0 was identified (rho = 0.115, $P = 0.601$). Of the large-scale networks explored in this study, the DAN, FPN and SMN had the highest percentage of voxels showing differences in CBF_0 (Table 4). No voxels with group-differences in basal perfusion were observed in the VN.

Table 3
Group-analysis of the sensorimotor parameters computed using the KINARM™ end-point robot (BKIN Technologies Ltd., Kingston, Ontario, Canada).

Object hit and avoid parameters	Healthy	mTBI	P value[a]
Distractor hits total	6.6 ± 8.5	7.3 ± 5.8	0.754
Hand bias hits (range: [-1 - 1])	0.1 ± 0.1	0.1 ± 0.1	0.448
Median error (%)	74.1 ± 7.0	73.2 ± 6.3	0.641
Object processing rate (objects/second)	2.7 ± 0.3	2.7 ± 0.2	0.725
Target hits total	172.4 ± 12.6	171.4 ± 7.3	0.777

Values are mean ± standard deviation.
[a] = Statistically compared using a univariate ANOVA. See (**Table 2**) for definition of each parameter.

3.3. Group-comparison of original and scaled functional connectivity matrices

Non-contiguous clustering of the gICA spatial components (Fig. 2) created a total of 41 ROIs spread across the 6 large-scale networks of interest (Table 4). The comparison of non-weighted FC coefficients from BOLD rs-fMRI between the groups showed significant differences ($P < 0.05$, corrected) within and across networks of the brain (Fig. 7A). A total of 29 seed-to-seed connections were different between the groups, of which 10 were from ROI pairs within networks, and 19 were from functional connections between networks. These included a mixture of both higher (Fig. 7A left, red) and lower seed-to-seed connectivity (Fig. 7A left, blue) in the mTBI group as compared to controls, which were distributed across a proportion of the networks studied. Specifically, differences in connectivity within the DMN, DAN and FNP were observed (Fig. 7A middle), while inter-network differences in the functional architecture of the cortical hubs included ROI pairs from the majority of the spatial components studied.

Because widespread differences in baseline perfusion were documented within the gICA functional components, FC coefficients were normalized by CBF_0 (see Fig. 4) in order to explore the possible differences in connectivity results after accounting for the effect of regional seed-based blood flow (Fig. 7B). When comparing the weighted FC coefficients between the groups, a reduced total of 14 seed-to-seed connections were identified that were different between the healthy and mTBI cohorts ($P < 0.05$, corrected). Significant differences in connectivity were documented within the FPN only, while previously observed group differences within the DMN and DAN (Fig. 7A middle) were no longer significant in this analysis (Fig. 7B middle). A number of inter-network connectivity differences between the DAN and the rest of the brain were still present after CBF_0 corrections, although many differences in seed-to-seed connections across networks including the DMN and SMN were not observed.

Lastly, a subset analysis of the co-localized results between differences in connectivity with the unweighted and CBF_0-weighted FC coefficient was done by multiplying the resultant statistical matrices together (Fig. 7C). The final combined matrix showed a total of 11 altered paired connections (6 with lower FC, 5 with higher FC) between the groups. Approximately 80% of these results were also identified with normalized FC (Fig. 7B). In other words, most connections highlighted in the CBF_0-scaled statistical analysis (Fig. 7B) were common to the unweighted differences in FC coefficients (Fig. 7A) between the groups. Only intra-network differences within the FPN (all showing lower FC in the mTBI) survived the weighted scaling and the matrix multiplication, while most of the inter-network significant differences involved the DAN (7/11 inter-network FC differences; Fig. 7C).

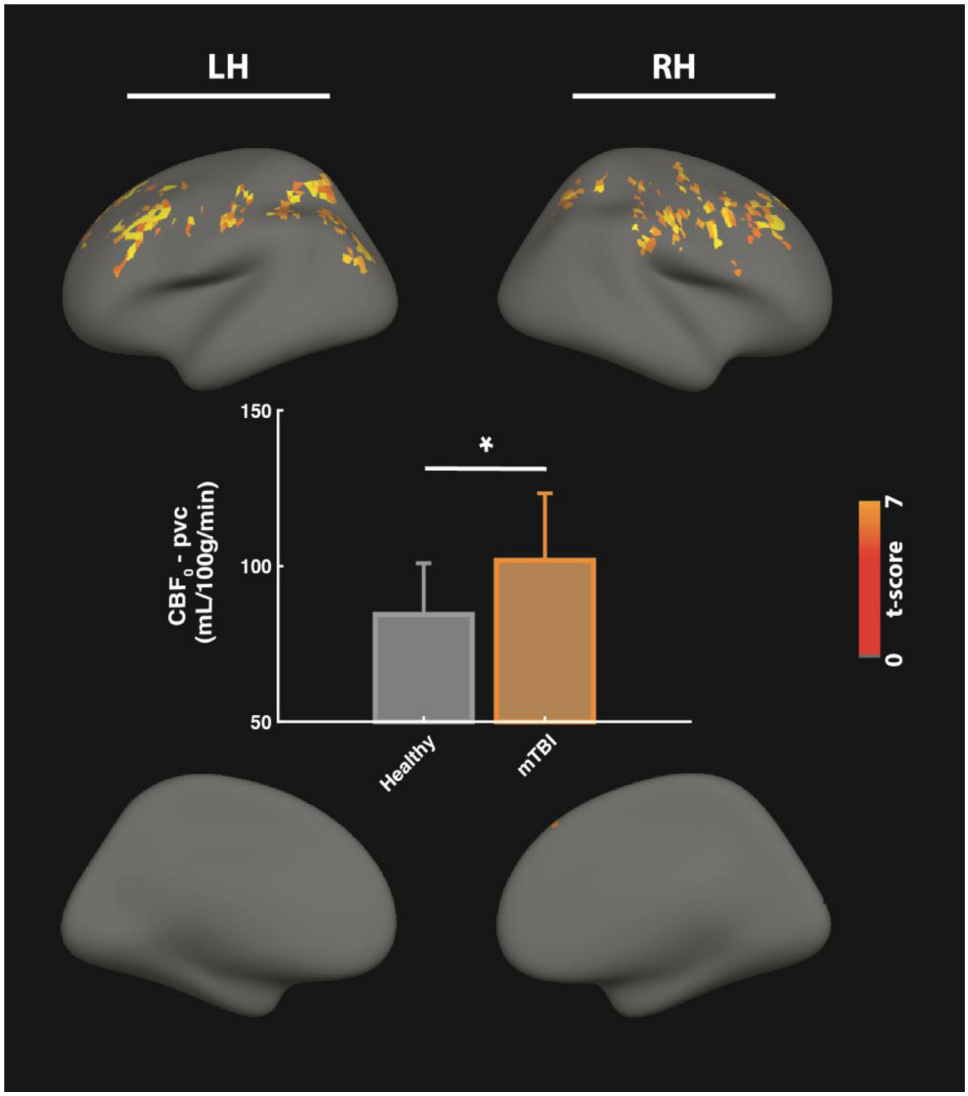

Fig. 6. Results from the voxelwise comparison of the perfusion maps between the groups. Significant clusters from the voxelwise analysis of the resting cerebral blood flow corrected for partial volume effects (CBF_0-pvc) maps which was restricted to voxels within the large-scale neural networks of interest described in Fig.3. Statistical group-comparisons were corrected for multiple comparisons at $P < 0.05$ using cluster sizes set to 94 voxels. The statistical maps are overlaid onto the freesurfer surface to show the lateral (top) and medial (bottom) views from the left (LH) and right (RH) hemispheres. The bar graph summarizes the mean value (± standard deviation) for the healthy and mTBI groups to show the magnitude and direction of the difference (* = $P < 0.05$, corrected) in CBF_0 within the region-of-interest (top).

4. Discussion

4.1. Main findings

In this study, we proposed a novel multi-modal approach inspired by (Qiu et al., 2017) to explore the effects of scaling FC coefficients by local physiology, which may be altered in patients with a history of mTBI. We are the first to implement such an approach as a way to combine information from rs-fMRI and cerebrovascular physiology to gather insight about the long-term effects of mTBI on brain FC biomarkers. The main findings in this study are three-fold: (1) Differences in CBF_0 within the spatial distribution of the large-scale networks were documented between the healthy and mTBI groups, although no significant differences in vascular reactivity (i.e., CVR) were observed. (2) Inter- and intra-network connectivity differences were documented between the healthy and mTBI participants, which is in line with previous work on the long-term effects of head injuries on brain connectivity (Doshi et al., 2015; Iraji et al., 2015; Mayer et al., 2011; Nathan et al., 2015; Rosenthal et al., 2018; Sours et al., 2015; Stevens et al., 2012; Xiong et al., 2016). Patterns of higher and lower synchronization between seed-to-seed connections were observed, especially in cortical hubs associated with the DMN, DAN and FPN. (3) Weighting of the connectivity matrices by CBF_0 measurements revealed fewer regions with significant differences in connectivity, although the majority of connections detected using the normalized analysis were spatially concordant with findings from the unscaled approach.

Table 4
Distribution of large-scale networks showing differences in baseline perfusion between the groups.

Network of interest	Total number of seeds	Total number of voxels (4mm isotropic)	% of voxels with differences in CBF_0
Dorsal attention network (DAN)	9	1559	34.8
Default mode network (DMN)	9	1600	4.8
Fronto-parietal network (FPN)	11	2274	39.2
Somatomotor network (SMN)	4	2019	34.1
Ventral attention network (VAN)	6	647	4.1
Vision network (VN)	2	1729	0

Network listed here are displayed in **Fig. 4** and labelled using the (Yeo et al., 2011) atlas. CBF_0 = baseline cerebral blood flow (mL/100g/min).

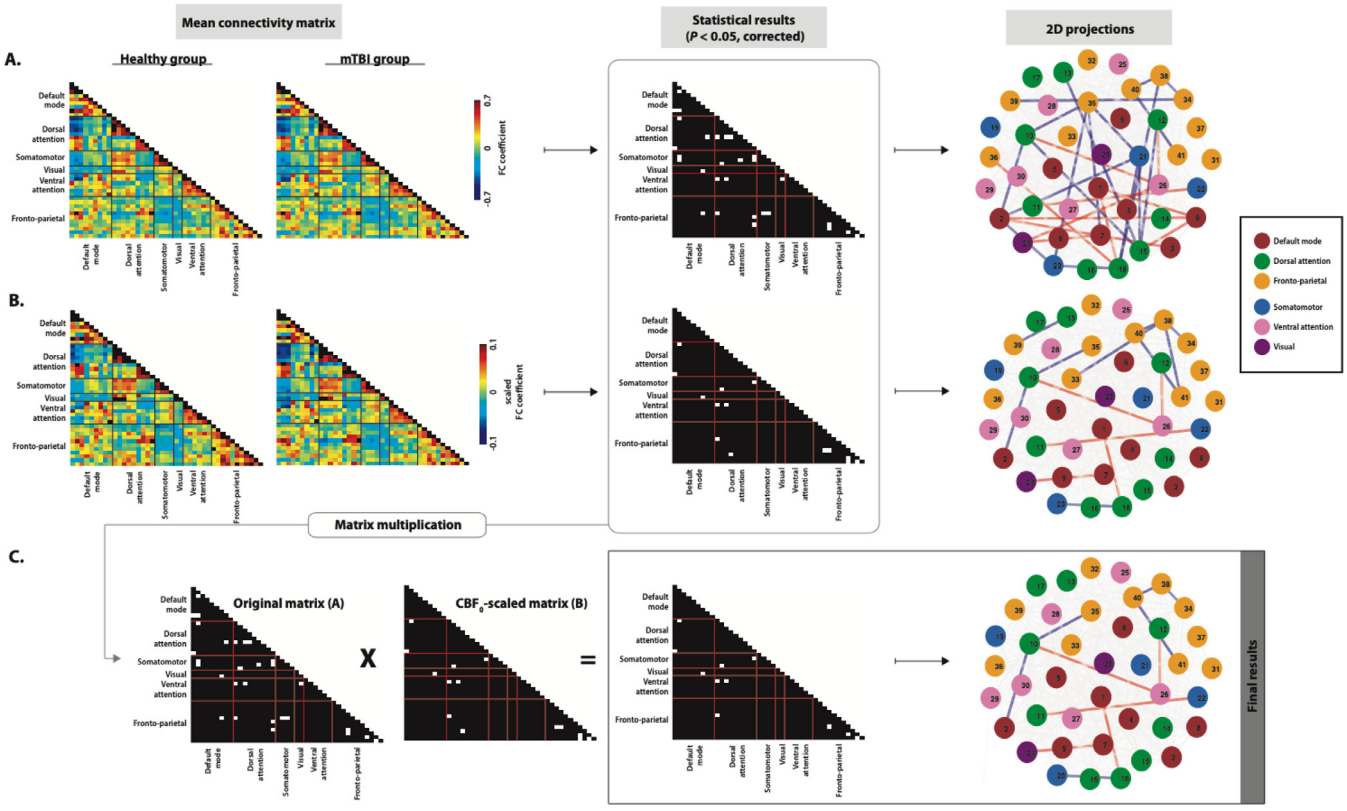

Fig. 7. Intra- and inter-network connectivity differences detected between the groups. The mean network connectivity matrices (left) for the healthy and mTBI group are displayed for each analysis conducted. These include the original connectivity matrices (non-weighted; (A)), and the normalized connectivity coefficients using seed-based resting cerebral blood flow (CBF_0; (B)) measurements. The binary statistical results (middle) showing seed-to-seed connections that differ significantly between the groups (white square), corrected for multiple comparison using a false discovery rate set to $P < 0.05$, were projected in 2D (right) using numbered nodes (colored based on the network labelling atlas (Yeo et al., 2011)) and connecting edges (links). Edges (light grey) for seed-to-seed connections showing significant differences between the groups following corrections for multiple comparisons were color-coded to show the direction of the group difference (blue = healthy > mTBI, red = healthy < mTBI). (C) Matrices from (A) and (B) were multiplied to extract intra- and inter-network connectivity differences that were robust to both the original and CBF_0-corrected analysis. The final calibrated 2D projections shows narrowed differences in network connectivity. (For interpretation of the references to color in this figure legend, the reader is referred to the web version of this article).

Altogether, these results suggest that although differences in the organization of large-scale network may follow mTBI, as previously reported, fluctuations in baseline physiology may confound the analysis of FC between groups (Chu et al., 2018; Liu, 2013). On the other hand, robust differences in network connectivity between functional nodes following correction for CBF_0 may provide evidence of reorganization of correlation structures across and within networks following mTBI. This process, referred to as cortical plasticity (Bashir et al., 2012; Meehan et al., 2017), could be a compensatory mechanism within the brain that allows for maintenance of sensorimotor function despite functional reorganization, as evidenced by equivalent performance on the sensorimotor task. Moving forward, the use of a multi-modal design combining BOLD and ASL imaging at rest may capture unique aspects of the changes in network connectivity and brain physiology that occur in functional networks of the brain post-mTBI.

4.2. Network-specific differences in baseline perfusion despite no differences in vascular reactivity

Voxelwise analysis of healthy and mTBI subjects demonstrated that CBF_0 may be chronically higher in certain regions of the brain for individuals with a history of head injury. Although the mechanisms for the pathogenesis of mTBI have yet to be elucidated, it has become apparent that changes in perfusion play an important role in the evolution of the biochemical sequelae that follows the injury in the short-term (Barkhoudarian et al., 2011; Churchill et al., 2017; Giza and Hovda, 2001, 2014), and throughout the long-term recovery process (Barlow et al., 2016; Mutch et al., 2016; Stephens et al., 2018). In the acute and sub-acute phases of post-mTBI, CBF_0 is typically reduced (Lin et al., 2016; Maugans et al., 2012; Meier et al., 2015; Wang et al., 2018, 2016), which reflects possible differences in cerebral metabolism at the cellular level (Champagne et al. (2020). *Under revision.*). In weeks and months following the injury, the opposite trend has been observed, with higher CBF_0 documented in patients recovering from mTBI compared to controls (Stephens et al., 2018), although findings of lower CBF_0 in chronic mTBI patients have also been reported (Wang et al., 2015). The results reported in this study are also consistent with reports of higher perfusion in patients with persistent mTBI-related symptomology (Barlow et al., 2016; Mutch et al., 2016; Stephens et al., 2018), which have been associated with the trajectory of recovery patterns, although no relationship between the higher CBF_0 and time post-mTBI was identified in our data. The variability in reports of altered CBF across different cohorts and the heterogeneity in the spatial distribution of CBF-based differences between groups post-mTBI emphasizes the need to account for possible subject-to-subject differences in perfusion, which could affect connectivity measurements from rs-fMRI (Chu et al., 2018; Liu, 2013).

In this study, no voxelwise differences in CVR within the spatial components of the gICA were identified. Widespread differences in CBF_0 without the presence of CVR-based differences suggests that the mechanisms associated with modulation of blood flow upon exposure to the vasodilatory HC stimulus were intact in the mTBI subjects

studied, at the group-level. Similar to CBF_0 findings from other studies, mixed results for differences in CVR post-mTBI have been reported (da Costa et al., 2016; Len et al., 2011; Len and Neary, 2011; Mutch et al., 2016). This heterogeneity in documented differences (or no differences) in vascular reactivity post-mTBI suggests that regional differences in cerebrovascular responsiveness to HC may be heterogeneous across patients where unique patient-specific signatures of changes in CVR occur post-injury (Mutch et al., 2016). It is also possible that the cohort studied did not differ in CVR both at the group- and subject-level, which has also been reported (da Costa et al., 2016). The wide variability in the time of injury post-mTBI studied may also preclude possible observation of differences in CVR between the groups, which emphasize the need for similar methods to be implemented in a large and more heterogenous patient population, moving forward. It is also important to consider that the analysis performed in this study was focused specifically on regions extracted from the gICA spatial components. CVR within other regions of the cerebral cortex outside of those may have been impaired (Ellis et al., 2016), although this is beyond the scope of this study, which was focused specifically on exploring the effects of impaired physiology on co-localized patterns of network connectivity following mTBI. Lastly, it should also be noted that the use of BOLD CVR may have limited our ability to identify differences in CVR, as the BOLD physiology reflects a compound effect that integrates changes in metabolism, blood volume and blood flow (Champagne et al., 2019a).

4.3. Network differences in brain network connectivity of large-scale networks and the effects of weighting in vascular physiology

In this study, BOLD rs-fMRI measurements of inter- and intra-network connectivity were used to compare the organization of cortical hubs in mTBI patients, relative to controls. Prior to normalization of the FC measurements using local physiological parameters, differences within and across large-scale network connectivity were identified, which were in line with the existing literature (Doshi et al., 2015; Iraji et al., 2015; Mayer et al., 2011; Nathan et al., 2015; Rosenthal et al., 2018; Sours et al., 2015; Stevens et al., 2012; Xiong et al., 2016). Patterns of higher and lower FC within the cortical networks of the injured group were observed which are also common in the study of brain network connectivity in mTBI patients (Iraji et al., 2015; Mayer et al., 2011; Sours et al., 2015; Stevens et al., 2012; Xiong et al., 2016). Consistent differences in connectivity markers post-mTBI based on the existing literature suggest that rs-fMRI may serve as a promising tool to understand the effects of head injuries on the organization of functional networks within the brain. Though most of the group-differences involved the DMN, DAN and FPN, altered seed-to-seed connections linking other networks such as the SMN, VN and VAN were also documented. This suggests that connectivity differences characterized by BOLD rs-fMRI post-mTBI may involve a wide range of ROIs across the GM. Additionally, the presence of group-differences in FC measurements despite the wide range of time since injury post-mTBI in this analysis suggests that differences in brain connectivity may persist long after injury.

In theory, alterations in BOLD-based FC after injury may be indicative of differences in the spontaneous synchronization of neurons associated with large-scale networks, local changes in perfusion, blood volume and oxidative metabolism (via neurocoupling mechanisms), or a combination of these factors, all of which effect the BOLD contrast (Fox and Raichle, 2007). Regional baseline physiological factors such as CBF_0 may also play an important role in the characterization of correlation structures based on activity of the brain at rest (Chu et al., 2018; Liu, 2013). This is because although FC is considered to be predominantly driven by neural activity (*reviewed in* Fox and Raichle, 2007), the synchrony of the BOLD time series across regions may also be dependent on vascular factors (Golestani et al., 2016) and physiological noise (Birn et al., 2006; Chang et al., 2009). In this study, widespread voxelwise differences in CBF_0 across the networks of interest motivated the approach to account for seed-based perfusion in the computation of FC coefficients. It is important to note that CBF_0 is not purely a vascular parameter, unlike CVR, in that it reflects a balance for the local vascular tone that is associated, at least in part, with the neuronal components at the cellular level (Liang et al., 2013). Thus, the weighing of CBF_0 in order to compare FC between patients with altered physiology assumes that neuronal firing driving the synchronization of the BOLD signal across cortical hubs is the major factor contributing to the computation of the FC coefficients, without the possible confounding effects of local changes in blood flow that are driven by vascular physiology (i.e., autoregulation) post-mTBI.

Co-localized differences in connectivity and perfusion have been reported previously in acute (Militana et al., 2016) and chronic (Sours et al., 2015) presentation of mTBI suggesting that the weighted method proposed in this study may provide valuable insight into the effects of mTBI on reorganization of cortical hubs, without the confounding nature of altered vascular parameters. Although calibrated results were narrowed to a more specific set of networks (**Fig. 7C**), robust differences within the FPN and between the DAN, the DMN and the rest of the brain provide possible evidence that the brain may reorganize after mTBI. More specifically, differences in intra- and inter-network FC including the DMN, DAN and SMN seem to have been the most affected by the scaling using CBF_0. These findings suggest that certain regions within the brain may share variance with respect to changes in perfusion and FC after mTBI, which may confound the direct analysis of connectivity across large-scale networks of brain. These systematic differences in physiology may be associated to direct changes in local physiology of the brain tissues, or a complex interaction involving multiple factors such as the ratio of large vessels to tissue volume, which has been shown to play a role in determining FC strength (Tak et al., 2015, 2014). These compensatory mechanisms may allow for proper cognitive, motor and sensory integration, which is supported by the fact that no group differences in the mTBI group were documented based on the OHA task, compared to controls.

Although the direct relationship between CBF_0 and FC has yet to be characterized in full, findings from (Chu et al., 2018) suggest that the degree of correlation between seeds within and across networks can be influenced by the complex relationship that relates physiological noise and neuronal activity, which together, make up the rs-fMRI BOLD contrast (*see* Fig.1 in Liu, 2013). This is because inter-voxel (or region) correlation coefficients with low influence from noise may be increased for regions with higher CBF_0, likely due elevated resting metabolism in neurons (Liang et al., 2013; Lord et al., 2013). Conversely, a negative association between CBF_0 and FC is also possible when the noise-related correlations (i.e., physiological processes and motion) dominate the FC coefficient (instead of being driven by neuronally-specific physiological modulators). Thus, the non-linear relationship between FC and CBF_0 arises from a balance between neurovascular coupling mechanisms linking CBF_0 and metabolic demand, and regional and global synchronization of neuronal activity (*see summary* Fig.13 in Chu et al., 2018). To support this contention, simulations from (Chu et al., 2018) showed that changes in perfusion can affect the FC measurements in ways that depend on both the local CBF_0 measurements, and the extent of the influence from physiological noise, which varies across cortical networks (Golestani et al., 2015). The same authors, and others (Tak et al., 2015), also showed that the presence of large vessels across selected regions of the brain may reduce FC despite local increases in CBF_0, which is likely associated with differences in the macrovascular content and local sources of physiological noise. Additional imaging of the vasculature using a time-of-flight sequence, as in (Tak et al., 2015), may help accounting for possible differences in resting macrovascular volume fraction across patients.

Taken together with findings from this study, it is possible that systemic physiological noise varying across regions of the brain (not neuronally specific modulators of the BOLD signal), along with

differences in baseline vascular physiology, may confound the computation of FC measurements and limit the ability for rs-fMRI to be used to identify group-level and individual-based differences due to mTBI. As reviewed in (Liu, 2013), the additional acquisition of electroencephalographic (EEG) or magnetoencephalographic (MEG) measurements may allow to complement our understanding of the confounding effects between baseline physiology and rs-fMRI findings. Strong correlations between rs-fMRI BOLD signal and EEG activity have been reported (de Munck et al., 2007; Goldman et al., 2002; Laufs et al., 2003; Moosmann et al., 2003), as well as with MEG recordings (Brookes et al., 2011; Liu et al., 2010), suggesting that future studies may consider multimodal imaging designs as a way to validate calibration methods such as the one proposed, and improve modeling of the potential changes in neural and vascular components that may characterize FC differences in clinical population.

4.4. Methodological limitations and future considerations

Despite the novelty of the imaging design and post-processing analysis proposed, the findings reported in this study are limited primarily by the large range of time post-injury used to make up the mTBI group. Although documented group-differences in both CBF_0 and network connectivity suggest that the brain may change following mTBI, future designs using this approach should use a narrower range of time since injury to provide better insight about the chronic effects of head injuries on cortical GM connectivity and physiology. The integration of longitudinal designs with multiple timepoints such as in (Nakamura et al., 2009) may also be an avenue to explore in order to understand the relationship between differences in vascular physiological parameters and functional markers of the brain throughout the recovery process in patients. Increasing the sample size of both groups in a larger study will also improve the power of the statistical analysis and the clinical applications of these findings.

The weighting approach employed in this study from (Qiu et al., 2017) assumes a linear relationship between the cerebrovascular physiology and its possible influence on the variability in network functional connectivity. As highlighted in recent studies by (Chu et al., 2018; Golestani et al., 2016), the physiological effects of CBF_0 and CVR may be better represented using a non-linear relationship, which reflects the increased complexity of the link between underlying vascular physiology and BOLD-based FC. Although no correction has yet been proposed to account for these possible non-linear relationships, with respect to comparing FC coefficients, future designs may consider alternative approaches to calibrate the resting-state BOLD signal. For instance, the acquisition of a rs-fMRI scan using a dual-echo pCASL sequence (Dai et al., 2008) may allow to calibrate the BOLD signal of the brain at rest with concurrent time-varying measurements of perfusion (Champagne et al., 2019b; Wu et al., 2009). This approach provides a comprehensive method to calibrate BOLD-based network connectivity measurements while accounting for different physiological modulators which contribute to the BOLD contrast. The use of dual-calibrated fMRI method, or QUO_2 MRI (Hoge, 2012), which incorporates both HC and hyperoxia breathing manipulations (Gauthier et al., 2012; Gauthier and Hoge, 2013), may also be implemented moving forward in order to compute additional hemodynamic parameters such as resting oxygen extraction fraction (OEF_0) and $CMRO_2$, in order to gain insight into the physiological mechanisms that underscore differences in blood flow following chronic mTBI.

In this study, the KINARM^{TM} end-point robot (BKIN Technologies Ltd., Kingston, Ontario, Canada) was used to assess the sensorimotor performance of the participants at the time of the MRI. Although the KINARM^{TM} may be an effective tool to provide objective measurements of the upper limb motor function and visuospatial skills (Bourke et al., 2016; Tyryshkin et al., 2014), it may be limited in its ability to assess specific neurocognitive functions typically reported following mTBI. Moving forward, the inclusion of a more comprehensive battery of tests such as the one used in (McCrea et al., 2013, 2003; Nelson et al., 2013) may help to better characterize possible differences in functional markers and their relationship to the symptomology of mTBI.

5. Conclusion

The primary objective of this study was to explore the effects of scaling vascular parameters in the comparison of rs-fMRI correlation structures between healthy and mTBI subjects. Inclusion of regional perfusion measurements in the computation of correlation coefficients within and across large-scale networks of the brain narrowed the differences in FC between the groups, suggesting that this approach may elucidate unique differences in connectivity post-mTBI while accounting for shared variance with CBF_0. Moving forward, this multimodal approach may improve the diagnostic and prognostic utilities of rs-fMRI in characterizing intrinsic pathological disturbances in the organization of cortical hubs within the brain. Moreover, this method may improve current data-driven classification models which have shown promising results in the characterization of mTBI using information from combined imaging modalities (Vergara et al., 2016). Altogether, the integration of multiple parameters with both vascular and neural origins, as well as the inclusion of comprehensive neurocognitive assessments, may help to identify the processes associated with cortical plasticity of the brain following mTBI and the patient-specific trajectories for recovery.

Funding

This work was supported with funding provided by Performance Phenomics.

Declaration of Competing of Interest

DJC is a founder of Performance Phenomics (PP). AR and CIM are employees of PP and AAC and NSC have received salary support from PP.

CRediT authorship contribution statement

Allen A. Champagne: Conceptualization, Data curation, Formal analysis, Methodology, Writing - original draft, Writing - review & editing. **Nicole S. Coverdale:** Conceptualization, Data curation, Funding acquisition, Methodology, Writing - review & editing. **Andrew Ross:** Conceptualization, Methodology, Writing - review & editing. **Yining Chen:** Conceptualization, Methodology, Writing - review & editing. **Christopher I. Murray:** Conceptualization, Methodology, Writing - review & editing. **David Dubowitz:** Conceptualization, Writing - review & editing. **Douglas J. Cook:** Funding acquisition, Supervision, Writing - review & editing.

Acknowledgments

The authors of this study would like to thank Mr Don Brien and Ms Janet Mirtle-Stroman for their dedication and willingness to help with the data collection. The authors would also like to thank Mr Boris Baker, Ms Kim Moore and Simone Appaqaq for their help with collecting the KINARM^{TM} data. Finally, we would like to thank Dr. J. J. Wang at UCLA for sharing the pCASL sequence used in this study.

References

A.K., F., M.E., S., M.D., A., E.B., M., 2018. Functional neurocognitive imaging to assess concussion biomarkers to treat dysregulation of neurovascular coupling in post-concussion syndrome. J. Neuroimaging.

Alsop, D.C., Detre, J.A., Golay, X., Gunther, M., Hendrikse, J., Hernandez-Garcia, L., Lu, H., Macintosh, B.J., Parkes, L.M., Smits, M., Van Osch, M.J.P., Wang, D.J.J., Wong, E.C., Zaharchuk, G., 2015. Recommended implementation of arterial spin-labeled

Perfusion mri for clinical applications: A consensus of the ISMRM Perfusion Study group and the European consortium for ASL in dementia. Magn. Reson. Med. 73, 102–116. https://doi.org/10.1002/mrm.25197.
Andersson, J.L.R., Jenkinson, M., Smith, S., 2007. Non-linear registration aka Spatial normalisation FMRIB Technial Report TR07JA2. Non-linear registration aka Spatial normalisation FMRIB Technial Report TR07JA2 22 In Pract.
Bandettini, P.A., Wong, E.C., 1997. A hypercapnia-based normalization method for improved spatial localization of human brain activation with fMRI. NMR Biomed. 10, 197–203. https://doi.org/10.1002/(SICI)1099-1492(199706/08)10:4/5<197::AID-NBM466>3.0.CO;2-S.
Barkhoudarian, G., Hovda, D.A., Giza, C.C., 2011. The molecular pathophysiology of concussive brain injury. Clin. Sports Med. 30, 33–48. vii–iii. https://doi.org/10.1016/j.csm.2010.09.001.
Barlow, K.M., Marcil, L.D., Dewey, D., Carlson, H.L., MacMaster, F.P., Brooks, B.L., Lebel, R.M., 2016. Cerebral perfusion changes in post-concussion syndrome: a prospective controlled cohort study. J. Neurotrauma. https://doi.org/10.1089/neu.2016.4634.
Bashir, S., Vernet, M., Yoo, W., ... 2012. Changes in cortical plasticity after mild traumatic brain injury. Restor. Neurol. 30, 277–282. https://doi.org/10.3233/RNN-2012-110207.Changes.
Beckmann, C.F., 2012. Modelling with independent components. Neuroimage. https://doi.org/10.1016/j.neuroimage.2012.02.020.
Birn, R.M., Diamond, J.B., Smith, M.A., Bandettini, P.A., 2006. Separating respiratory-variation-related fluctuations from neuronal-activity-related fluctuations in fMRI. Neuroimage. https://doi.org/10.1016/j.neuroimage.2006.02.048.
Bourke, T.C., Lowrey, C.R., Dukelow, S.P., Bagg, S.D., Norman, K.E., Scott, S.H., 2016. A robot-based behavioural task to quantify impairments in rapid motor decisions and actions after stroke. J. Neuroeng. Rehabil. 1–13. https://doi.org/10.1186/s12984-016-0201-2.
Brookes, M.J., Hale, J.R., Zumer, J.M., Stevenson, C.M., Francis, S.T., Barnes, G.R., Owen, J.P., Morris, P.G., Nagarajan, S.S., 2011. Measuring functional connectivity using MEG: methodology and comparison with fcMRI. Neuroimage https://doi.org/10.1016/j.neuroimage.2011.02.054.
Burnett, T., Bishop, S., Wallace, C., Wright, S., Neary, P., Ainslie, P., Van Donkelaar, P., 2014. Pathophysiology of sport-related concussion injuries: Interrelationships between physiology, neurocognitive and subjective symptom changes. Brain Inj. https://doi.org/10.3109/02699052.2014.892379.
Champagne, A.A., Bhogal, A.A., Coverdale, N.S., Mark, C.I., Cook, D.J., 2017. A novel perspective to calibrate temporal delays in cerebrovascular reactivity using hypercapnic and hyperoxic respiratory challenges. Neuroimage 11.
Champagne, A.A., Coverdale, N.S., Germuska, M., Cook, D.J., 2019a. Multi-parametric analysis reveals metabolic and vascular effects driving differences in BOLD-based cerebrovascular reactivity associated with a history of sport concussion. Brain Inj. 33, 1479–1489. https://doi.org/10.1080/02699052.2019.1644375.
Champagne, A.A., Coverdale, N.S., Nashed, J.Y., Fernandez-Ruiz, J., Cook, D.J., 2019b. Resting CMRO 2 fluctuations show persistent network hyper-connectivity following exposure to sub-concussive collisions. NeuroImage Clin. 22, 101753. https://doi.org/10.1016/j.nicl.2019.101753.
Champagne A.A., Coverdale N.S., Ross A., Chen Y., Murray C.I., Dubowitz D., Cook D.J., 2020. Multi-modal normalization of resting-state using local physiology reduces changes in functional connectivity patterns observed in mTBI patients. NeuroImage: Clinical. [Accepted; In press]. 2020.
Chang, C., Cunningham, J.P., Glover, G.H., 2009. Influence of heart rate on the BOLD signal: the cardiac response function. Neuroimage. https://doi.org/10.1016/j.neuroimage.2008.09.029.
Chappell, M.A., Groves, A.R., MacIntosh, B.J., Donahue, M.J., Jezzard, P., Woolrich, M.W., 2011. Partial volume correction of multiple inversion time arterial spin labeling MRI data. Magn. Reson. Med. 65, 1173–1183. https://doi.org/10.1002/mrm.22641.
Chappell, M.A., Groves, A.R., Whitcher, B., Woolrich, M.W., 2009. Variational Bayesian inference for a nonlinear forward model. IEEE Trans. Signal Process. 57, 223–236. https://doi.org/10.1109/TSP.2008.2005752.
Chen, G., Adleman, N.E., Saad, Z.S., Leibenluft, E., Cox, R.W., 2014. Applications of multivariate modeling to neuroimaging group analysis: A comprehensive alternative to univariate general linear model. Neuroimage 99, 571–588. https://doi.org/10.1016/j.neuroimage.2014.06.027.
Chu, P.P.W., Golestani, A.M., Kwinta, J.B., Khatamian, Y.B., Chen, J.J., 2018. Characterizing the modulation of resting-state fMRI metrics by baseline physiology. Neuroimage. https://doi.org/10.1016/j.neuroimage.2018.02.004.
Churchill, N.W., Hutchison, M.G., Richards, D., Leung, G., Graham, S.J., Schweizer, T.A., 2017. The first week after concussion: Blood flow, brain function and white matter microstructure. NeuroImage Clin. 14, 480–489. https://doi.org/10.1016/j.nicl.2017.02.015.
Concussion in Sport Group, 2013. Sport concussion assessment tool - 3rd edition. Br. J. Sports Med.
Cox, R., 1996. AFNI : software for analysis and visualization of functional magnetic resonance neuroimages. Comput. Biomed. Res. 29, 162–173.
Cox, R.W., Chen, G., Glen, D.R., Reynolds, R.C., Taylor, P.A., 2017. FMRI clustering in AFNI: false-positive rates redux. Brain Connect. 7, 152–171. https://doi.org/10.1089/brain.2016.0475.
Cox, R.W., Reynolds, R.C., Taylor, P.A., 2016. AFNI and clustering: false positive rates redux. bioRxiv. https://doi.org/10.1101/065862.
da Costa, L., van Niftrik, C.B., Crane, D., Fierstra, J., Bethune, A., 2016. Temporal profile of cerebrovascular reactivity impairment, gray matter volumes, and persistent symptoms after mild traumatic head injury. Front. Neurol. 7, 1–10. https://doi.org/10.3389/fneur.2016.00070.
Dai, W., Garcia, D., De Bazelaire, C., Alsop, D.C., 2008. Continuous flow-driven inversion for arterial spin labeling using pulsed radio frequency and gradient fields. Magn. Reson. Med. 60, 1488–1497. https://doi.org/10.1002/mrm.21790.
Dall'Acqua, P., Johannes, S., Mica, L., Simmen, H.-P., Glaab, R., Fandino, J., Schwendinger, M., Meier, C., Ulbrich, E.J., Müller, A., Baetschmann, H., Jäncke, L., Hänggi, J., 2017. Functional and structural network recovery after mild traumatic brain injury: a 1-year longitudinal study. Front. Hum. Neurosci. https://doi.org/10.3389/fnhum.2017.00280.
Davis, T.L., Kwong, K.K., Weisskoff, R.M., Rosen, B.R., 1998. Calibrated functional MRI: mapping the dynamics of oxidative metabolism. Proc. Natl. Acad. Sci. USA 95, 1834–1839. https://doi.org/10.1073/pnas.95.4.1834.
de Munck, J.C., Gonçalves, S.I., Huijboom, L., Kuijer, J.P.A., Pouwels, P.J.W., Heethaar, R.M., Lopes da Silva, F.H., 2007. The hemodynamic response of the alpha rhythm: an EEG/fMRI study. Neuroimage. https://doi.org/10.1016/j.neuroimage.2007.01.022.
Donahue, M.J., Strother, M.K., Lindsey, K.P., Hocke, L.M., Tong, Y., deB Frederick, B., 2016. Time delay processing of hypercapnic fMRI allows quantitative parameterization of cerebrovascular reactivity and blood flow delays. J. Cereb. Blood Flow Metab. 36, 1767–1779. https://doi.org/10.1177/0271678X15608643.
Doshi, H., Wiseman, N., Liu, J., Wang, W., Welch, R.D., O'Neil, B.J., Zuk, C., Wang, X., Mika, V., Szaflarski, J.P., Haacke, E.M., Kou, Z., 2015. Cerebral hemodynamic changes of mild traumatic brain injury at the acute stage. PLoS One. https://doi.org/10.1371/journal.pone.0118061.
Ellis, M.J., Ryner, L.N., Sobczyk, O., Fierstra, J., Mikulis, D.J., Fisher, J.A., Duffin, J., Mutch, W.A.C., 2016. Neuroimaging assessment of cerebrovascular reactivity in concussion: current concepts, methodological considerations, and review of the literature. Front. Neurol. 7, 1–16. https://doi.org/10.3389/fneur.2016.00061.
Fisher, J.A., Venkatraghavan, L., Mikulis, D.J., 2018. Magnetic resonance imaging–based cerebrovascular reactivity and hemodynamic reserve. Stroke STROKEAHA 118.021012. https://doi.org/10.1161/STROKEAHA.118.021012.
Fox, M.D., Raichle, M.E., 2007. Spontaneous fluctuations in brain activity observed with functional magnetic resonance imaging. Nat. Rev. Neurosci. https://doi.org/10.1038/nrn2201.
Gauthier, C.J., Desjardins-Crépeau, L., Madjar, C., Bherer, L., Hoge, R.D., 2012. Absolute quantification of resting oxygen metabolism and metabolic reactivity during functional activation using QUO2 MRI. Neuroimage 63, 1353–1363. https://doi.org/10.1016/j.neuroimage.2012.07.065.
Gauthier, C.J., Hoge, R.D., 2013. A generalized procedure for calibrated MRI incorporating hyperoxia and hypercapnia. Hum. Brain Mapp. 34, 1053–1069. https://doi.org/10.1002/hbm.21495.
Giza, C.C., Hovda, D.a., 2001. The neurometabolic cascade of concussion. J. Athl. Train. 36, 228–235. https://doi.org/10.1227/NEU.0000000000000505.
Giza, C.C., Hovda, D.A., 2014. The new neurometabolic cascade of concussion. Neurosurgery 75, S24–S33. https://doi.org/10.1227/NEU.0000000000000505.
Goldman, R.I., Stern, J.M., Engel, J., Cohen, M.S., 2002. Simultaneous EEG and fMRI of the alpha rhythm. Neuroreport. https://doi.org/10.1097/00001756-200212200-00022.
Golestani, A.M., Chang, C., Kwinta, J.B., Khatamian, Y.B., Jean Chen, J., 2015. Mapping the end-tidal CO2 response function in the resting-state BOLD fMRI signal: Spatial specificity, test-retest reliability and effect of fMRI sampling rate. Neuroimage. https://doi.org/10.1016/j.neuroimage.2014.10.031.
Golestani, A.M., Kwinta, J.B., Strother, S.C., Khatamian, Y.B., Chen, J.J., 2016. The association between cerebrovascular reactivity and resting-state fMRI functional connectivity in healthy adults: The influence of basal carbon dioxide. Neuroimage 132, 301–313. https://doi.org/10.1016/j.neuroimage.2016.02.051.
Greve, D.N., Fischl, B., 2009. Accurate and robust brain image alignment using boundary-based registration. Neuroimage 48, 63–72. https://doi.org/10.1016/j.neuroimage.2009.06.060.
Griffanti, L., Douaud, G., Bijsterbosch, J., Evangelisti, S., Alfaro-Almagro, F., Glasser, M.F., Duff, E.P., Fitzgibbon, S., Westphal, R., Carone, D., Beckmann, C.F., Smith, S.M., 2017. Hand classification of fMRI ICA noise components. Neuroimage 154, 188–205. https://doi.org/10.1016/j.neuroimage.2016.12.036.
Griswold, M.A., Jakob, P.M., Heidemann, R.M., Nittka, M., Jellus, V., Wang, J., Kiefer, B., Haase, A., 2002. Generalized autocalibrating partially parallel acquisitions (GRAPPA). Magn. Reson. Med. https://doi.org/10.1002/mrm.10171.
Hoge, R., Atkinson, J., Gill, B., Crelier, G., Marrett, S., 1999. Investigation of BOLD signal dependence on cerebral blood flow and oxygen consumption: The …. Magn. Reson. Med. 863, 849–863.
Hoge, R.D., 2012. Calibrated fMRI. Neuroimage. https://doi.org/10.1016/j.neuroimage.2012.02.022.
Iraji, A., Benson, R.R., Welch, R.D., O'Neil, B.J., Woodard, J.L., Ayaz, S.I., Kulek, A., Mika, V., Medado, P., Soltanian-Zadeh, H., Liu, T., Haacke, E.M., Kou, Z., 2015. Resting state functional connectivity in mild traumatic brain injury at the acute stage: independent component and seed-based analyses. J. Neurotrauma. https://doi.org/10.1089/neu.2014.3610.
Jenkinson, M., Bannister, P., Brady, M., Smith, S., 2002. Improved optimization for the robust and accurate linear registration and motion correction of brain images. Neuroimage 17, 825–841. https://doi.org/10.1016/S1053-8119(02)91132-8.
Jenkinson, M., Beckmann, C.F., Behrens, T.E.J., Woolrich, M.W., Smith, S.M., 2012a. Fsl. Neuroimage 62, 782–790. https://doi.org/10.1016/j.neuroimage.2011.09.015.
Jenkinson, M., Beckmann, C.F., Behrens, T.E.J., Woolrich, M.W., Smith, S.M., 2012b. Fsl. Neuroimage 62, 782–790. https://doi.org/10.1016/j.neuroimage.2011.09.015.
Lajoie, I., Tancredi, F.B., Hoge, R.D., 2016. Regional reproducibility of BOLD calibration parameter M, OEF and resting-state CMRO2 measurements with QUO2 MRI. PLoS One 11, 31. https://doi.org/10.1371/journal.pone.0163071.
Laufs, H., Kleinschmidt, A., Beyerle, A., Eger, E., Salek-Haddadi, A., Preibisch, C., Krakow, K., 2003. EEG-correlated fMRI of human alpha activity. Neuroimage. https://doi.org/10.1016/S1053-8119(03)00286-6.

Len, T.K., Neary, J.P., 2011. Cerebrovascular pathophysiology following mild traumatic brain injury. Clin. Physiol. Funct. Imaging. https://doi.org/10.1111/j.1475-097X.2010.00990.x.

Len, T.K., Neary, J.P., Asmundson, G.J.G., Goodman, D.G., Bjornson, B., Bhambhani, Y.N., 2011. Cerebrovascular reactivity impairment after sport-induced concussion. Med. Sci. Sports Exerc 43, 2241–2248. https://doi.org/10.1249/MSS.0b013e3182249539.

Liang, X., Zou, Q., He, Y., Yang, Y., 2013. Coupling of functional connectivity and regional cerebral blood flow reveals a physiological basis for network hubs of the human brain. Proc. Natl. Acad. Sci. 110, 1929–1934. https://doi.org/10.1073/pnas.1214900110.

Lin, C.M., Tseng, Y.C., Hsu, H.L., Chen, C.J., Chen, D.Y.T., Yan, F.X., Chiu, W.T., 2016. Arterial spin labeling perfusion study in the patients with subacute mild traumatic brain injury. PLoS One. https://doi.org/10.1371/journal.pone.0149109.

Little, C.E., Emery, C., Black, A., Scott, S.H., Meeuwisse, W., Nettel-Aguirre, A., Benson, B., Dukelow, S., 2015. Test-retest reliability of KINARM robot sensorimotor and cognitive assessment: in pediatric ice hockey players. J. Neuroeng. Rehabil. 12, 78. https://doi.org/10.1186/s12984-015-0070-0.

Liu, P., B. De Vis, J., Lu, H., 2018. Cerebrovascular reactivity (CVR) MRI with CO2 challenge: a technical review. Neuroimage 1–12. https://doi.org/10.1016/j.neuroimage.2018.03.047.

Liu, P., Hebrank, A.C., Rodrigue, K.M., Kennedy, K.M., Park, D.C., Lu, H., 2013. A comparison of physiologic modulators of fMRI signals. Hum. Brain Mapp. 34, 2078–2088. https://doi.org/10.1002/hbm.22053.

Liu, T.T., 2013. Neurovascular factors in resting-state functional MRI. Neuroimage 80, 339–348. https://doi.org/10.1016/j.neuroimage.2013.04.071.

Liu, Z., Fukunaga, M., de Zwart, J.A., Duyn, J.H., 2010. Large-scale spontaneous fluctuations and correlations in brain electrical activity observed with magnetoencephalography. Neuroimage. https://doi.org/10.1016/j.neuroimage.2010.01.092.

Lord, L.D., Expert, P., Huckins, J.F., Turkheimer, F.E., 2013. Cerebral energy metabolism and the brain's functional network architecture: An integrative review. J. Cereb. Blood Flow Metab. https://doi.org/10.1038/jcbfm.2013.94.

Lovell, M.R., Pardini, J.E., Welling, J., Collins, M.W., Bakal, J., Lazar, N., Roush, R., Eddy, W.F., Becker, J.T., 2007. Functional brain abnormalities are related to clinical recovery and time to return-to-play in athletes. Neurosurgery 61, 352–359. https://doi.org/10.1227/01.NEU.0000279985.94168.7F.

Mark, C.I., Slessarev, M., Ito, S., Han, J., Fisher, J.a., Pike, G.B., 2010. Precise control of end-tidal carbon dioxide and oxygen improves BOLD and ASL cerebrovascular reactivity measures. Magn. Reson. Med. 64, 749–756. https://doi.org/10.1002/mrm.22405.

Jenkinson, Mark, Bannister, Peter, 2002. Improved methods for the registration and motion correction of brain images. Neuroimage 17, 825–841.

Maugans, T.A., Farley, C., Altaye, M., Leach, J., Cecil, K.M., 2012. Pediatric sports-related concussion produces cerebral blood flow alterations. Pediatrics 129, 28–37. https://doi.org/10.1542/peds.2011-2083.

Mayer, A.R., Mannell, M.V., Ling, J., Gasparovic, C., Yeo, R.A., 2011. Functional connectivity in mild traumatic brain injury. Hum. Brain Mapp. 32, 1825–1835. https://doi.org/10.1002/hbm.21151.

McCrea, M., Guskiewicz, K., Randolph, C., Barr, W.B., Hammeke, T.A., Marshall, S.W., Powell, M.R., Woo Ahn, K., Wang, Y., Kelly, J.P., 2013. Incidence, clinical course, and predictors of prolonged recovery time following sport-related concussion in high school and college athletes. J. Int. Neuropsychol. Soc. 19, 22–33. https://doi.org/10.1017/S1355617712000872.

McCrea, M., Guskiewicz, K.M., Marshall, S.W., Barr, W., Randolph, C., Cantu, R.C., Onate, J.A., Yang, J., Kelly, J.P., 2003. Acute effects and recovery time following concussion in collegiate football players: the NCAA Concussion Study. Jama 290, 2556–2563. https://doi.org/10.1001/jama.290.19.2556.

McCrory, P., Meeuwisse, W.H., Aubry, M., Cantu, R.C., Dvorák, J., Echemendia, R.J., Engebretsen, L., Johnston, K.M., Kutcher, J.S., Raftery, M., Sills, A., Benson, B.W., Davis, G.a., Ellenbogen, R., Guskiewicz, K.M., Herring, S.a., Iverson, G.L., Jordan, B.D., Kissick, J., McCrea, M., McIntosh, A.S., Maddocks, D.L., Makdissi, M., Purcell, L., Putukian, M., Schneider, K., Tator, C.H., Turner, M., 2013. In: Consensus Statement on Concussion in Sport-The 4th International Conference on Concussion in Sport Held in Zurich, November 2012. 5. PM R, pp. 255–279. https://doi.org/10.1016/j.pmrj.2013.02.012.

Meehan, S.K., Mirdamadi, J.L., Martini, D.N., Broglio, S.P., 2017. Changes in cortical plasticity in relation to a history of concussion during adolescence. Front. Hum. Neurosci. https://doi.org/10.3389/fnhum.2017.00005.

Meier, T.B., Brummel, B.J., Singh, R., Nerio, C.J., Polanski, D.W., Bellgowan, P.S.F., 2015. The underreporting of self-reported symptoms following sports-related concussion. J. Sci. Med. Sport 18, 507–511. https://doi.org/10.1016/j.jsams.2014.07.008.

Militana, A.R., Donahue, M.J., Sills, A.K., Solomon, G.S., Gregory, A.J., Strother, M.K., Morgan, V.L., 2016. Alterations in default-mode network connectivity may be influenced by cerebrovascular changes within 1 week of sports related concussion in college varsity athletes: a pilot study. Brain Imaging Behav. 10, 559–568. https://doi.org/10.1007/s11682-015-9407-3.

Moosmann, M., Ritter, P., Krastel, I., Brink, A., Thees, S., Blankenburg, F., Taskin, B., Obrig, H., Villringer, A., 2003. Correlates of alpha rhythm in functional magnetic resonance imaging and near infrared spectroscopy. Neuroimage. https://doi.org/10.1016/S1053-8119(03)00344-6.

Murphy, K., Birn, R.M., Bandettini, P.A., 2013. Resting-state fMRI confounds and cleanup. Neuroimage 80, 349–359. https://doi.org/10.1016/j.neuroimage.2013.04.001.

Mutch, W., Ellis, A.C., Ryner, M.J., Graham, L.N., Dufault, R., Gregson, B., Brian, Hall, Bunge, T., Martin. Essig, M., 2016. Brain magnetic resonance imaging CO2 stress testing in adolescent post-concussion syndrome: pCASL findings. J. Neurosurg 125, 525–786. https://doi.org/10.3171/2015.6.JNS15972.

Nakamura, T., Hillary, F.G., Biswal, B.B., 2009. Resting network plasticity following brain injury. PLoS One. https://doi.org/10.1371/journal.pone.0008220.

Nathan, D.E., Oakes, T.R., Yeh, P.H., French, L.M., Harper, J.F., Liu, W., Wolfowitz, R.D., Wang, B.Q., Graner, J.L., Riedy, G., 2015. Exploring variations in functional connectivity of the resting state default mode network in mild traumatic brain injury. Brain Connect. 5, 102–114. https://doi.org/10.1089/brain.2014.0273.

Nelson, Janecek, J.K., McCrea, M.A., 2013. Acute clinical recovery from sport-related concussion. Neuropsychol. Rev. https://doi.org/10.1007/s11065-013-9240-7.

Ogawa, S., Lee, T.M., Kay, A.R., Tank, D.W., 1990. Brain magnetic resonance imaging with contrast dependent on blood oxygenation. Proc. Natl. Acad. Sci. USA 87, 9868–9872. https://doi.org/10.1073/pnas.87.24.9868.

Ogawa, S., Menon, R.S., Tank, D.W., Kim, S.G., Merkle, H., Ellermann, J.M., Ugurbil, K., 1993. Functional brain mapping by blood oxygenation level-dependent contrast magnetic resonance imaging. A comparison of signal characteristics with a biophysical model. Biophys. J. https://doi.org/10.1016/S0006-3495(93)81441-3.

Para, A.E., Sam, K., Poublanc, J., Fisher, J.A., Crawley, A.P., Mikulis, D.J., 2017. Invalidation of fMRI experiments secondary to neurovascular uncoupling in patients with cerebrovascular disease. J. Magn. Reson. Imaging. https://doi.org/10.1002/jmri.25639.

Poublanc, J., Crawley, A.P., Sobczyk, O., Montandon, G., Sam, K., Mandell, D.M., Dufort, P., Venkatraghavan, L., Duffin, J., Mikulis, D.J., Fisher, J.a, 2015. Measuring cerebrovascular reactivity: the dynamic response to a step hypercapnic stimulus. J. Cereb. Blood Flow Metab 1–11. https://doi.org/10.1038/jcbfm.2015.114.

Prisman, E., Slessarev, M., Han, J., Poublanc, J., Mardimae, A., Crawley, A., Fisher, J., Mikulis, D., 2008. Comparison of the effects of independently-controlled end-tidal PCO(2) and PO(2) on blood oxygen level-dependent (BOLD) MRI. J. Magn. Reson. Imaging 27, 185–191. https://doi.org/10.1002/jmri.21102.

Qiu, M., Scheinost, D., Ramani, R., Constable, R.T., 2017. Multi-modal analysis of functional connectivity and cerebral blood flow reveals shared and unique effects of propofol in large-scale brain networks. Neuroimage 148, 130–140. https://doi.org/10.1016/j.neuroimage.2016.12.080.

Rosenthal, S., Gray, M., Fatima, H., Sair, H.I., Whitlow, C.T., 2018. Functional MR Imaging: Blood Oxygen Level–Dependent and Resting State Techniques in Mild Traumatic Brain Injury. Neuroimaging Clin. N. Am. https://doi.org/10.1016/j.nic.2017.09.008.

Scott, S.H., 1999. Apparatus for measuring and perturbing shoulder and elbow joint positions and torques during reaching. J. Neurosci. Methods 89, 119–127.

Smith, S.M., Brady, J.M., 1997. SUSAN—a new approach to low level image processing. Int. J. Comput. Vis. 23, 45–78. https://doi.org/10.1023/A:1007963824710.

Sours, C., Zhuo, J., Roys, S., Shanmuganathan, K., Gullapalli, R.P., 2015. Disruptions in resting state functional connectivity and cerebral blood flow in mild traumatic brain injury patients. PLoS One 10. https://doi.org/10.1371/journal.pone.0134019.

Stephens, J.A., Liu, P., Lu, H., Suskauer, S.J., 2018. Cerebral blood flow after mild traumatic brain injury: associations between symptoms and post-injury perfusion. J. Neurotrauma. https://doi.org/10.1089/neu.2017.5237.

Stevens, M.C., Lovejoy, D., Kim, J., Oakes, H., Kureshi, I., Witt, S.T., 2012. Multiple resting state network functional connectivity abnormalities in mild traumatic brain injury. Brain Imaging Behav. 6, 293–318. https://doi.org/10.1007/s11682-012-9157-4.

Tak, S., Polimeni, J.R., Wang, D.J.J., Yan, L., Chen, J.J., 2015. Associations of resting-state fMRI functional connectivity with flow-BOLD coupling and regional vasculature. Brain Connect 5, 137–146. https://doi.org/10.1089/brain.2014.0299.

Tak, S., Wang, D.J.J., Polimeni, J.R., Yan, L., Chen, J.J., 2014. Dynamic and static contributions of the cerebrovasculature to the resting-state BOLD signal. Neuroimage 84, 672–680. https://doi.org/10.1016/j.neuroimage.2013.09.057.

Tyryshkin, K., Coderre, A.M., Glasgow, J.I., Herter, T.M., Bagg, S.D., Dukelow, S.P., Scott, S.H., 2014. A robotic object hitting task to quantify sensorimotor impairments in participants with stroke. J. Neuroeng. Rehabil. 11, 47. https://doi.org/10.1186/1743-0003-11-47.

Vergara, Victor M., Mayer, A.R., Damaraju, E., Hutchison, K., Calhoun, V.D., 2017. The effect of preprocessing pipelines in subject classification and detection of abnormal resting state functional network connectivity using group ICA. Neuroimage. https://doi.org/10.1016/j.neuroimage.2016.03.038.

Vergara, V.M., Mayer, A.R., Damaraju, E., Kiehl, K.A., Calhoun, V., 2016. Detection of mild traumatic brain injury by machine learning classification using resting state functional network connectivity and fractional anisotropy. J. Neurotrauma. https://doi.org/10.1089/neu.2016.4526.

Vergara, V.M., Mayer, A.R., Damaraju, E., V.D., C., 2017. The effect of preprocessing in dynamic functional network connectivity used to classify mild traumatic brain injury. Brain Behav. https://doi.org/10.1002/brb3.809.

Vergara, V.M., Mayer, A.R., Kiehl, K.A., Calhoun, V.D., 2018. Dynamic functional network connectivity discriminates mild traumatic brain injury through machine learning. NeuroImage Clin. https://doi.org/10.1016/j.nicl.2018.03.017.

Wang, Y., Nelson, L.D., LaRoche, A.A., Pfaller, A.Y., Nencka, A.S., Koch, K.M., McCrea, M.A., 2016. Cerebral blood flow alterations in acute sport-related concussion. J. Neurotrauma 33, 1227–1236. https://doi.org/10.1089/neu.2015.4072.

Wang, Y., Nencka, A.S., Meier, T.B., Guskiewicz, K., Mihalik, J.P., Brooks, M.A., Saykin, A.J., Koch, K.M., Wu, Y., Nelson, L.D., Mcallister, T.W., Broglio, S.P., Mccrea, M.A., 2018. Cerebral blood flow in acute concussion : preliminary ASL findings from the NCAA-DoD CARE consortium. Brain Imaging Behav. 1–11. https://doi.org/10.1007/s11682-018-9946-5.

Wang, Y., West, J.D., Bailey, J.N., Westfall, D.R., Xiao, H., Arnold, T.W., Kersey, P.A., Saykin, A.J., McDonald, B.C., 2015. Decreased cerebral blood flow in chronic pediatric mild TBI: an MRI perfusion study. Dev Neuropsychol 40, 40–44. https://doi.org/10.1080/87565641.2014.979927.

Wu, C.W., Gu, H., Lu, H., Stein, E.A., Chen, J.H., Yang, Y., 2009. Mapping functional

connectivity based on synchronized CMRO2 fluctuations during the resting state. Neuroimage 45, 694–701. https://doi.org/10.1016/j.neuroimage.2008.12.066.
Xiong, K.L., Zhang, J.N., Zhang, Y.L., Zhang, Y., Chen, H., Qiu, M.G., 2016. Brain functional connectivity and cognition in mild traumatic brain injury. Neuroradiology. https://doi.org/10.1007/s00234-016-1675-0.
Yeo, B.T.T., Krienen, F.M., Sepulcre, J., Sabuncu, M.R., Lashkari, D., Hollinshead, M., Roffman, J.L., Smoller, J.W., Zollei, L., Polimeni, J.R., Fischl, B., Liu, H., Buckner, R.L., 2011. The organization of the human cerebral cortex estimated by intrinsic functional connectivity. J. Neurophysiol. 106, 1125–1165. https://doi.org/10.1152/jn.00338.2011.
Zhang, Y., Brady, M., Smith, S., 2001. Segmentation of brain MR images through a hidden Markov random field model and the expectation-maximization algorithm. IEEE Trans Med Imaging 20, 45–57. https://doi.org/10.1109/42.906424.